Jet Properties from $\pi^0 - h^\pm$ and $h^\pm - h^\pm$ Correlations in $d + Au$ and $p + p$ collisions

N. Grau, P. Constantin, J. G. Lajoie, C. A. Ogilvie, O. Ohia, J. Rak

October 11, 2004

Abstract

This analysis note outlines the analysis done post-Quark Matter 2004 updating the fixed-p_T $h^\pm - h^\pm$ correlation analysis outlined in Ref. [1] and the recent analysis of $\pi^0 - h^\pm$ correlations. Instead of correlation functions we create conditional yield distributions and extract not only the width information from those but also jet conditional yields. We have also analyzed the Run-3 p+p data as well. We report on the associated-p_T, trigger-p_T, centrality, and x_E dependence of the various jet properties, $\langle j_{Ty} \rangle$, $\langle z \rangle \langle k_{Ty} \rangle$, dN/dp_T, and dN/dx_E.

Contents

List of Figures

List of Tables

1 π^0 Reconstruction

1.1 ERT photon triggers

In the analysis of the $\pi^0 - h^{\pm}$ correlations, we have used the entire set of ERT photon triggers used in Run3 d+Au and p+p data sets. A detailed outline of the ERT trigger is found in [2]. We can see the effect on the high-p_T π^0's by plotting the ratio of π^0 p_T spectra in a MinBias sample and the ERT triggered sample. Fig. 1 is such a plot for the d+Au runs. In this case we see a factor of ~ 100 increase in the high-p_T π^0.

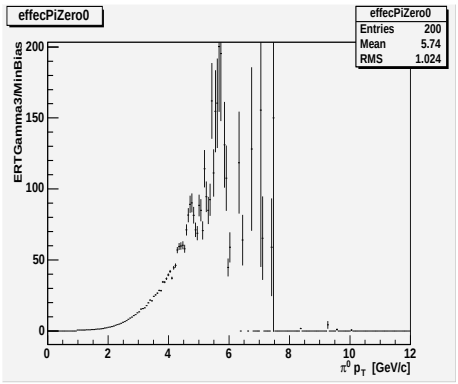

Figure 1: Ratio of π^0 ERT_Gamma3 triggered p_T spectrum to MinBias p_T spectrum in d+Au.

1.2 EmCal Time of Flight

A run-by-run time of flight correction is done for the EmCal. The time of flight, with the BBC t_0 subtracted, distribution is accumulated for each run and fit with a gaussian. The means and widths are stored and used for the time of flight cut. This was first employed for the Run2 Au+Au analysis. An example time of flight distribution is in Fig.2

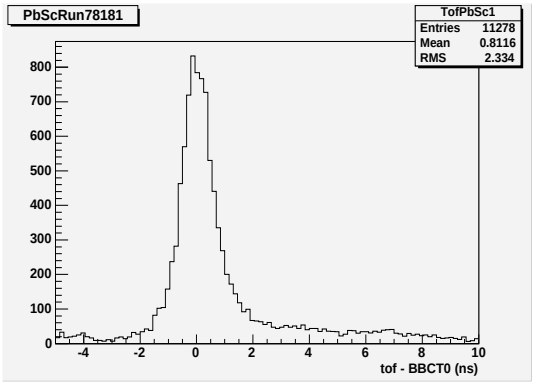

Figure 2: Example of Run 78181 PbSc EmCal tof-BBC t_0

1.3 π^0 Invariant Mass

The following photon cuts were made to select good quality photons:

- $E_{cluster} > 0.5GeV$

- $\chi^2 < 3$
- tof within 2 σ of the fitted mean

From this list of good photon candidates we create invariant mass plots with only a cut on the asymmetry of the photon energies, $\alpha < 0.7$. We combine photons from both PbSc and PbGl and between PbSc and PbGl. These invariant mass distributions for different p_T are shown in Fig. 3

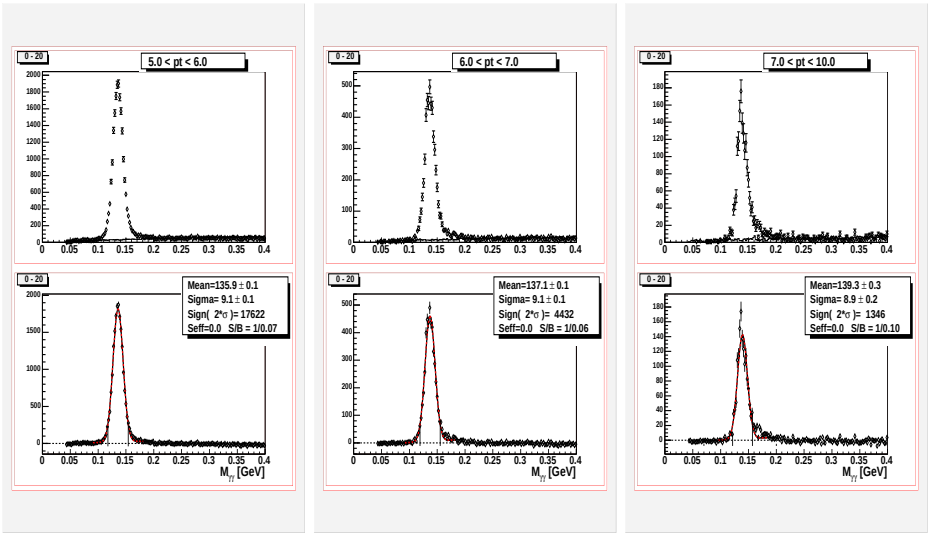

Figure 3: 0-20% central d+Au π^0 invariant mass of good pairs of photons with an energy asymmetry cut of $\alpha < 0.7$. The upper plots are the signal and normalized background. The background in normalized between $0.2 - 0.3$ GeV. The lower plots are background subtracted.

The signal-to-background ratio (Fig. 4) is quite large above 3 GeV. Because of the large S/B, we have little to no background contribution in the correlations. The background contribution will be taken into account as a systematic error. For the our candidate π^0's, we cut on 2 σ around the mean of the gaussian fits to the subtracted invariant mass spectra (lower plots of Fig.3). The means and widths of the π^0 mass are a function of p_T. We have parameterized the upper (mean+2σ) and lower mass (mean-2σ) limits as a function of p_T and centrality with a second-order polynomial. The upper and lower mass cuts for each centrality bin are plotted in Fig. 5.

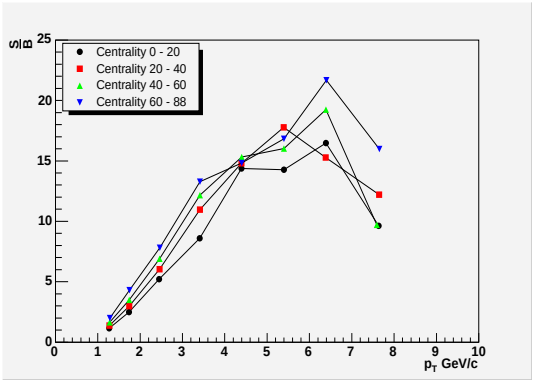

Figure 4: π^0 candidate S/B vs. p_T for different d+Au centrality

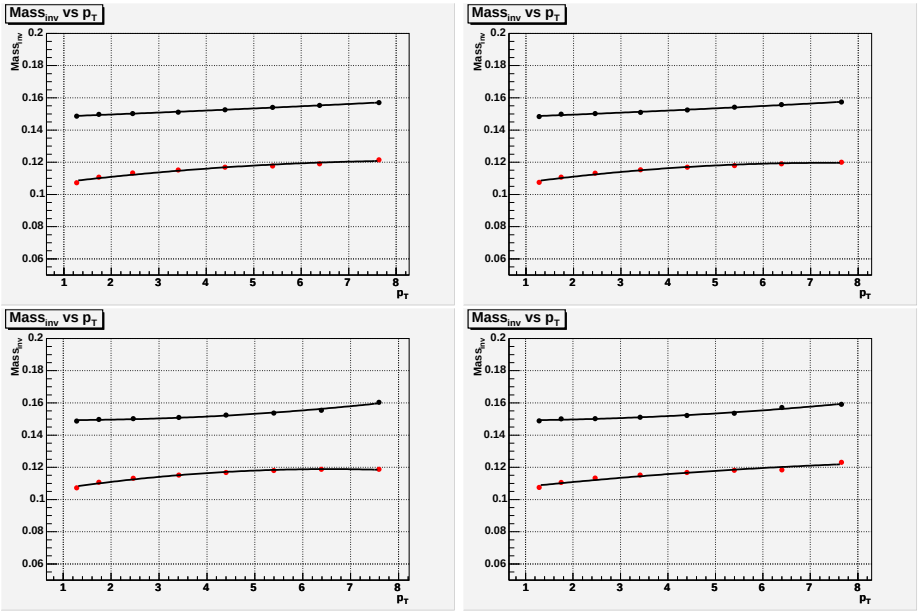

Figure 5: Upper and lower mass bounds as a function of p_T for of the centrality for the d+Au dataset. Upper left, 0-20%, upper right, 20-40%, lower left, 40-60%, lower right, 60-88%. Black points are 2σ above the mean and the red points are 2σ below the mean. The line represents a second-order polynomial fit to parameterize these curves.

2 Conditional Yields

2.1 Constructing Conditional Yields

In the initial $h^{\pm} - h^{\pm}$ analysis we constructed correlation functions and, because of an arbitrary normalization, only extracted the shape of the distribution. But by an appropriate normalization we can convert the correlations functions to unsubtracted conditional yield distributions. In this way we not only have the same shape information but also the conditional yield values. The following few lines outline the procedure to normalize.

We know that

$$\frac{1}{N_{trig}}\frac{dN^{pair}}{d\Delta\phi} \propto \frac{Real(\Delta\phi)}{Mix(\Delta\phi)} \tag{1}$$

We integrate both sides in order to get the appropriate normalization of the real/mix ratio. This gives us

$$\frac{1}{N_{trig}}\frac{dN^{pair}}{d\Delta\phi} = \frac{N^{pair}}{N_{trig}}\frac{R_{\Delta\eta}/\epsilon_{assoc}}{\int \frac{Real(\Delta\phi)}{Mix(\Delta\phi)}}\frac{Real(\Delta\phi)}{Mix(\Delta\phi)} \tag{2}$$

where ϵ_{assoc} is the associated single particle efficiency and $R_{\Delta\eta}$ is the eta correction for the jet yield. In all cases the associated particles are hadrons and their efficiency (versus p_T and centrality) was determined in AN [3]. The $\Delta\eta$ correction is outlined in the $d + Au$ $\pi^{\pm} - h^{\pm}$ AN [4].

The single particle efficiency, 1/Correction Function(CF), was parameterized as

$$\begin{aligned} \mathrm{CF}_{\mathrm{west}} &= 4.17/p_T + 20.56 - 0.34p_T + 0.015p_T^2 \\ \mathrm{CF}_{\mathrm{east}} &= 3.5/p_T + 18.47 - 0.147p_T - 0.0029p_T^2 \end{aligned} \tag{3}$$

where these CF's were obtained for the following cuts: $|zed| < 40$ cm, each arm corrected to 2π in azimuth, and $|\eta| < 0.5$. For this analysis there are a couple of corrections based on the cuts applied. We take an arithmetic mean of the CFs. Since each arm is corrected for 2π, we have a factor of 1/2 for the azimuthal acceptance. We correct to $|\eta| < 0.35$ - a factor of 0.7. The *zed* range we use is $|zed| < 75$ cm - a factor of 0.53.

We can fit these Conditional Yield distributions with a flat term and two gaussians

$$\frac{1}{N_{trig}}\frac{dN^{pair}}{d\Delta\phi} = N + \frac{S_N}{\sqrt{2\pi}\sigma_N}e^{\frac{-\Delta\phi^2}{2\sigma_N^2}} + \frac{S_F}{\sqrt{2\pi}\sigma_F}e^{\frac{-(\Delta\phi-\pi)^2}{2\sigma_F^2}} \tag{4}$$

Therefore, there are 5 fit parameters. Further S_F and S_N have the interpretation as the jet-correlation areas and thus represent the pair yield per trigger particle in the near and far angle. The fixed-p_T correlations are fit with this equation using MINOS.

The $\pi^0 - h^{\pm}$ correlations at high-p_T have low statistics. As such we fit with the log-likelihood methods as outlined in J. Jia's analysis note [4]. If we multiply both sides of Eqn.4 by the Mixed distribution and divide by the normalization constant one finds

$$Real(\Delta\phi) = \left(N + \frac{S_N}{\sqrt{2\pi}\sigma_N}e^{\frac{-\Delta\phi^2}{2\sigma_N^2}} + \frac{S_F}{\sqrt{2\pi}\sigma_F}e^{\frac{-(\Delta\phi-\pi)^2}{2\sigma_F^2}}\right)\frac{Mix(\Delta\phi)}{\frac{N^{pair}}{N_{trig}}\frac{R_{\Delta\eta}/\epsilon_{assoc}}{\int \frac{Real(\Delta\phi)}{Mix(\Delta\phi)}}} \tag{5}$$

So we fit the real distribution by the above fit function and scale the yields by the normalization constant. In this way, we can use a log-likelihood fit since the real distribution statistics has a Poissonian distribution within each bin.

2.2 Fixed-p_T $h^{\pm} - h^{\pm}$

All cuts made on the hadrons are the same as in the initial analysis([1]). Fig. 17 in Appendix B shows the fixed-p_T $h^{\pm} - h^{\pm}$ conditional yield distribution as constructed with Eqn. 2.

2.3 Assorted $\pi^0 - h^{\pm}$

We have performed two sets of correlations each on the p+p and d+Au datasets. The first is to keep the trigger π^0 constant and vary the associated hadron p_T. From these correlations we create x_E distributions where x_E is defined as

$$x_E = \frac{\vec{p}_{T,trig} \cdot \vec{p}_{T,assoc}}{p^2_{T,trig}} \tag{6}$$

The d+Au conditional yield distributions for the fixed trigger data are found in Appendix E.

In the second study we fix the associated hadron p_T and vary the π^0 trigger. The π^0 trigger p_T are broken up into $5-6-7-10$ GeV while the associated hadron is from $2-5$ GeV. The d+Au $\pi^0 - h^{\pm}$ distributions are found in Appendix C. The p+p results for $\pi^0 - h^{\pm}$ correlations for the equivalent binning in d+Au is found in Appendix G.

3 Results

3.1 Fixed-p_T

The $h^{\pm} - h^{\pm}$ fixed-p_T distributions, fitted with Eqn. 4, have two guassian widths which are related to $\langle|j_{\perp y}|\rangle$, the fragmentation momentum perpendicular to the jet axis, and $\langle z\rangle\langle|k_{\perp y}|\rangle$, the di-jet acoplanarity. The equations used to find $\langle|j_{\perp y}|\rangle$ and $\langle z\rangle\langle|k_{\perp y}|\rangle$ are

$$\langle|j_{\perp y}|\rangle = \langle p_{\perp}\rangle \cdot \sin\frac{\sigma_N}{\sqrt{\pi}} \tag{7}$$

$$\langle|k_{\perp y}|\rangle\langle z\rangle = \langle p_{\perp}\rangle\sqrt{\frac{1}{2}\sin^2\left(\sqrt{\frac{2}{\pi}}\sigma_F\right) - \sin^2\left(\sqrt{\frac{1}{\pi}}\sigma_N\right)} \tag{8}$$

where Eqn. 7 and Eqn. 8 are for a single component. They can be related to the RMS by multiplying by $\sqrt{\frac{\pi}{2}}$.

It was also found that the fits to the conditional yield distributions can have considerable asymmetric errors. These were found from MINOS and are quoted here. The systematic errors were found in the same way as the previous analysis. We varied some of the cuts (the fiducial cut, ghost removal, and drift chamber pair cuts) and took the systematic error as the maximum extent of those points from the nominal values. There is an additional systematic error due to the assumptions placed on the formula derivation which are included only on $\langle|j_{\perp y}|\rangle$ and $\langle z\rangle\langle|k_{\perp y}|\rangle$. There is a 10% normalization error that is included in the systematic errors of the yields.

Fig. 6 shows the near and far angle widths and $\langle|j_{\perp y}|\rangle$ and $\langle z\rangle\langle|k_{\perp y}|\rangle$ as a function of p_T with the asymmetric statistical and systematic errors. We can find the weighted average of the $\langle|j_{\perp y}|\rangle$ and $\langle|k_{\perp y}|\rangle$ for p_T above 1.5 GeV.

$$\langle|j_{Ty}|\rangle = 0.3760^{+0.0132+0.0054}_{-0.0119-0.0028} \quad \text{GeV/c} \tag{9}$$

$$\langle z\rangle\langle|k_{Ty}|\rangle = 0.7446^{+0.0602+0.0688}_{-0.0489-0.0939} \quad \text{GeV/c} \tag{10}$$

For comparison the preliminary values were

$$\langle|j_{Ty}|\rangle = 0.369 \pm 0.013(stat.)^{+0.005}_{-0.015}(sys.) \quad \text{GeV/c} \tag{11}$$

$$\langle z\rangle\langle|k_{Ty}|\rangle = 0.747 \pm 0.064(stat.)^{+0.001}_{-0.057}(sys.) \quad \text{GeV/c} \tag{12}$$

The values are within the statistical errors.

Fig. 7 is a plot of the conditional yields. To correctly count the conditional yield you include all pairs of non-similar particles. Therefore, you will overcount the actual number of distinguishable pairs. This is done so that the number of trigger particles is the number of single particles in the p_T bin. For example, say there are 3 particles in a given fixed-p_T bin. There are 3 distinct pairs for those 3 particles: 1+2, 1+3, and 2+3. But each of the particles in that bin will have 2 associated particles. The correct way to count that would be to count every pair that a given particle has: 1 – 1+2, 1+3; 2– 2+1, 2+3; 3 – 3+1, 3+2. The total pairs are 6 in that case and the number of triggers are 3. So the ratio $\frac{N^{pairs}}{N_{trig}} = 2$ which is what it should be.

We have also measured the x_E distribution of particles from the away side. These x_E distributions are plotted in Appendix B. These x_E distributions were fit with a Landau function. The extracted value of x_E was the maximum of the fit. Plotting the away side conditional yield as a function of x_E would produce something close to a fragmentation function. In this case, both particles are within the same p_T bin and, since we change both trigger and associated p_T we are not sampling a single fragmentation function. What we do measure is a convolution of each of the p_T bins fragmentation function. Therefore, we should not expect that the slope of such a distribution should be ~ -6 as for vacuum fragmentation. For the fixed-p_T far-side conditional yield vs. x_E we have a slope of -14.792 ± 1.266.

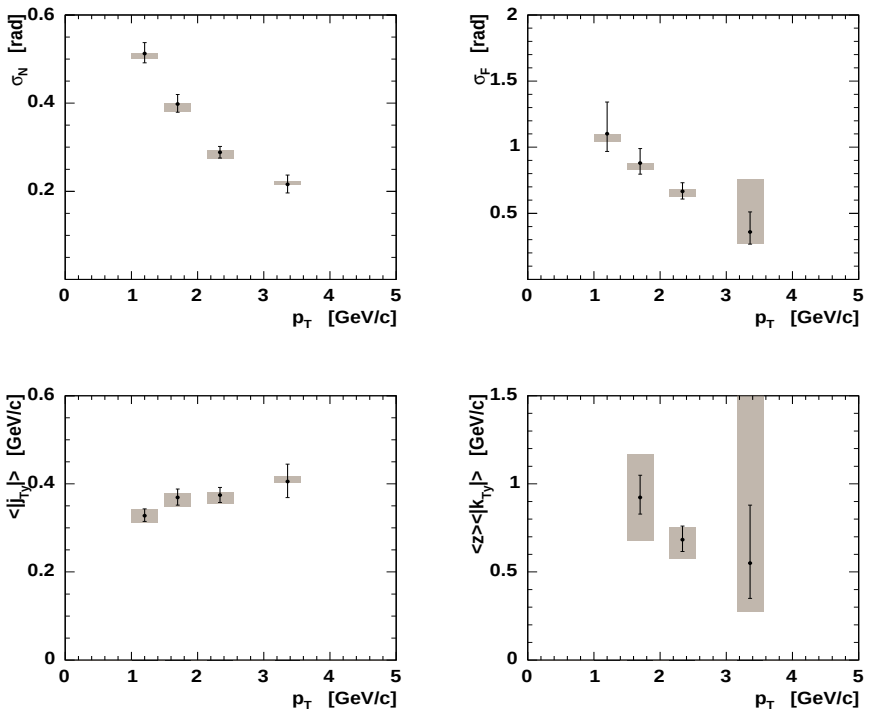

Figure 6: Fixed-p_T $h^{\pm} - h^{\pm}$ shape analysis results. Upper left, σ_N, upper right, σ_F, lower left, $\langle |j_{\perp y}| \rangle$, lower right, $\langle z \rangle \langle |k_{\perp y}| \rangle$ as a function of p_T. The systematic errors are maximum extent by varying some of the analysis cuts. The values are for the figure are found in Table 3 Appendix B

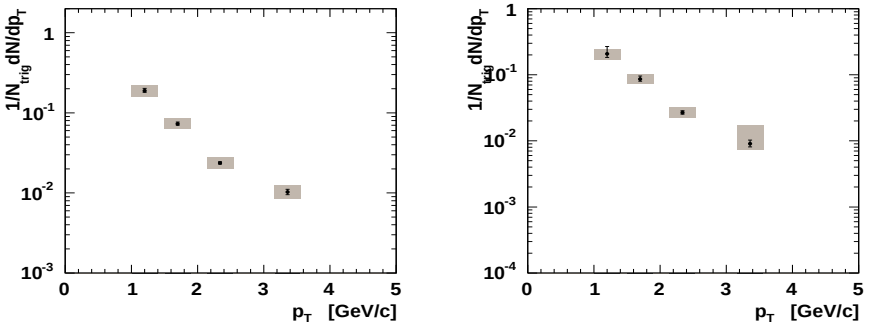

Figure 7: Fixed-p_T $h^{\pm} - h^{\pm}$ conditional yields. Near angle conditional yield (left), Far angle conditional yield (right). Values are given in Table 4 in Appendix B

3.2 Assorted-p_T $\pi^0 - h^{\pm}$

The $\pi^0 - h^{\pm}$ conditional yield distributions were fit with Eqn. 5. The extracted widths are then related to $\langle |j_{\perp y}| \rangle$ and $\langle z \rangle \langle |k_{\perp y}| \rangle$.

$$\langle |j_{Ty}| \rangle = \sqrt{\frac{2}{\pi}} \sigma_N \frac{\langle p_{T,\pi^0} \rangle \langle p_{T,h} \rangle}{\sqrt{\langle p_{T,\pi^0} \rangle^2 + \langle p_{T,h} \rangle^2}} \tag{13}$$

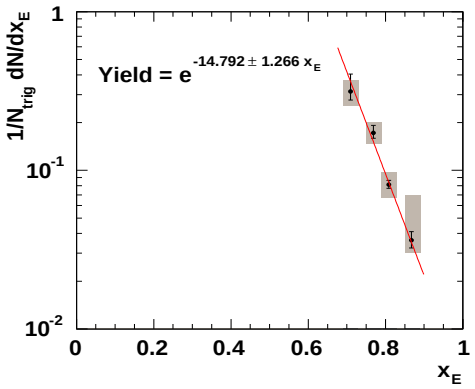

Figure 8: Far-angle jet conditional yield vs. x_E. The fit is an exponential.

$$\langle |k_{Ty}| \rangle \langle z \rangle = \langle p_{T,\pi^0} \rangle \sqrt{\frac{1}{2}\sin^2\left(\sqrt{\frac{2}{\pi}}\sigma_F\right) - \frac{1}{2}\left(\frac{\langle |j_{\perp y}| \rangle}{\langle p_{T,h} \rangle}\right)^2 (1 + x_h^2)} \tag{14}$$

$x_h = \langle p_{T,h} \rangle / \langle p_{T,\pi^0} \rangle$.

3.2.1 Systematic Error Determination

For these assorted $\pi^0 - h^\pm$ correlations a contributing systematic is the background contribution to the yields and widths. Using a toy Monte Carlo, several π^0's were generated per event with a give jet-like correlation with several hadrons. The π^0's were decayed with some of the photons removed from the event. π^0's were then reconstructed and correlated with the hadrons. The correlation distribution for real, reconstructed π^0's, fake, reconstructed π^0's, and for the real + fake reconstructed π^0's are given in Fig. 9. From the fits using Eqn. 4 we find the relationship between the signal, background, and measured widths and yields

$$\frac{S\sigma_{N,sig} + B\sigma_{N,bkg}}{S+B} = \sigma_{N,meas} \tag{15}$$

$$Y_{N,sig} + Y_{N,bkg} = Y_{N,meas} \tag{16}$$

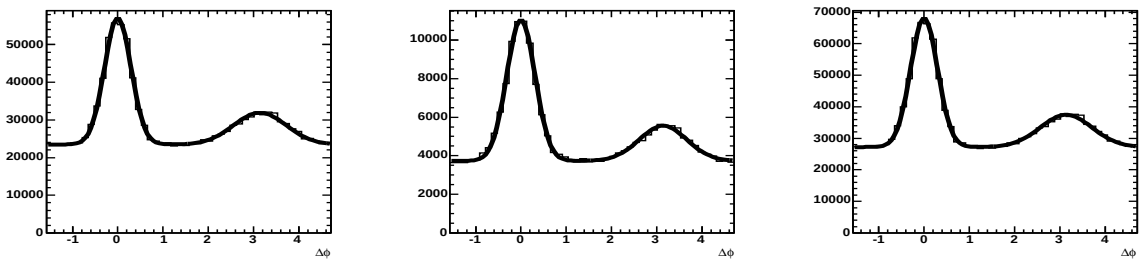

Figure 9: Toy Monte Carlo results for real, reconstructed $\pi^0 - h^\pm$ correlations (left), fake, reconstructed $\pi^0 - h^\pm$ correlations (center), and total $\pi^0 - h^\pm$ correlations(right). Black line is a two gaussian fit to the distributions to determine the relationship between measured, background, and signal widths and yields.

To apply these relations, the width and the yield in for the background π^0's needed to be estimated. To do this we used results from correlations of photon pairs outside the π^0 mass bin with hadrons. From the widths and the yields from three bins outside the π^0 mass, 0.05-0.1 GeV, 0.220-0.3 GeV, and 0.3-0.4 GeV, we extrapolated the background yield and width. Fig. 10 shows an example of the width and yield extraction. The systematic error was taken as the correction due to the background contribution as calculated with Eqn. 15.

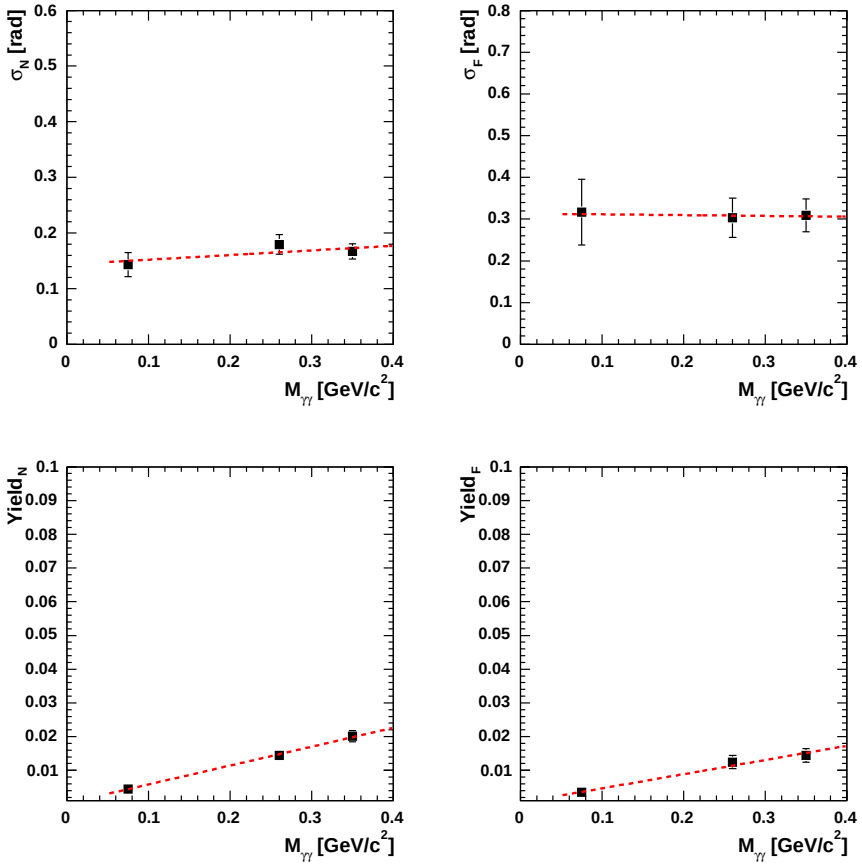

Figure 10: Extraction of the background yields and widths outside the π^0 mass bin. The fits are lines to the data and the background values are evaluated at the π^0 mass of 130 GeV/c^2

As with the $h^{\pm} - h^{\pm}$ analysis, we have varied some of the cuts to determine a systematic error for the extracted widths and the areas. We did not remove ghost tracks from the event pool, we removed the "internal" drift chamber fiducial cut, and increased the pi0 decay asymmetry cut to α <0.8. Each of these were varied separately. The maximum extent was taken for all p_T and was not different between p+p and d+Au.

A further systematic error on the extracted $\langle|j_{\perp y}|\rangle$ and $\langle z\rangle\langle|k_{\perp y}|\rangle$, is evaluated by the validity of the assumptions in the derivation of the formulas. J. Jia [4] independently derived a set of formulas for $\langle|j_{\perp y}|\rangle$ and $\langle z\rangle\langle|k_{\perp y}|\rangle$with less strict assumptions. The difference between the two formula is taken as another systematic error on the $\langle|j_{\perp y}|\rangle$ and $\langle z\rangle\langle|k_{\perp y}|\rangle$. The final systematic error on the yields is the efficiency calculation which is 10% normalization error for all yields. Table 1 outlines the table of systematic error values.

type	$\frac{\Delta\sigma_N}{\sigma_N}$	$\frac{\Delta\sigma_F}{\sigma_F}$	$\frac{\Delta S_N}{S_N}$	$\frac{\Delta S_F}{S_F}$
Cut variation	4%	3%	3%	3%
S/B correction	1-3%	1-3%	1%	1-5%
normalization	N/A	N/A	10%	10%
total	4.1-5%	3.2-4.2%	10.5%	10.5-11.7%
type			$\frac{\Delta\langle\|j_{Ty}\|\rangle}{\langle\|j_{Ty}\|\rangle}$	$\frac{\Delta\langle z\rangle\langle\|k_{Ty}\|\rangle}{\langle z\rangle\langle\|k_{Ty}\|\rangle}$
Approximation to Eqns			5%	4%
total			6.5-7.1%	$\sim 5\%$

Table 1: Systematic Errors for $\pi^0 - h^{\pm}$ correlation results for all d+Au centralities and p+p.

3.2.2 Constant Associated Hadron $p_T$in d+Au and p+p

The near and far angle widths and the extracted $\langle|j_{\perp y}|\rangle$ and $\langle z\rangle\langle|k_{\perp y}|\rangle$ are plotted in Fig. 11 for the centrality integrated d+Au data and p+p data. The centrality dependence of these quantities are plotted in Fig. 12. There is no obvious difference between the p+p and the d+Au data and no clear centrality dependence either.

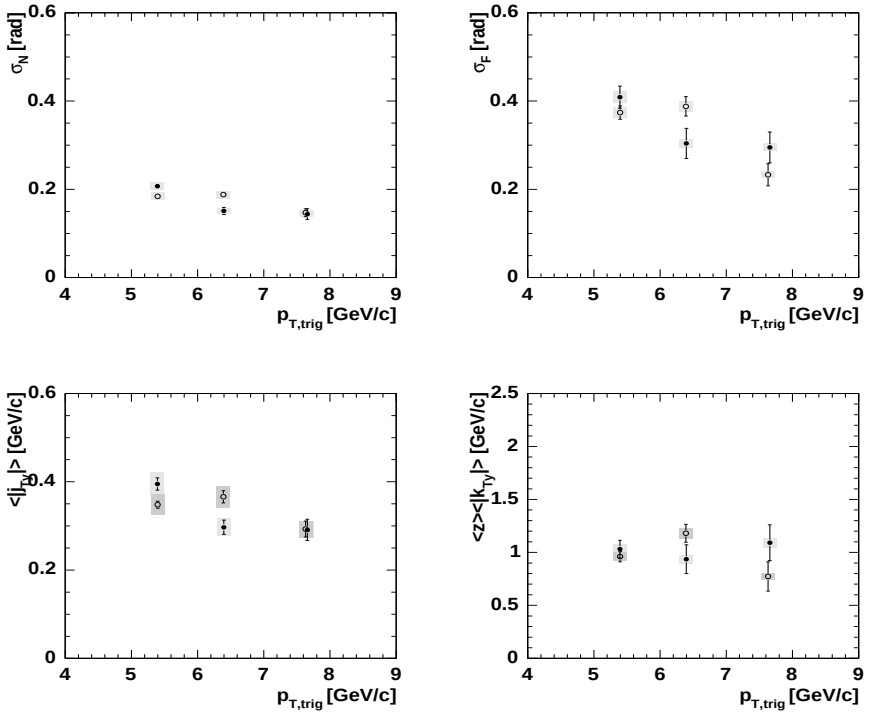

Figure 11: The extracted near angle width (upper left), far angle width (upper right), $\langle|j_{\perp y}|\rangle$ (lower left), and $\langle z\rangle\langle|k_{\perp y}|\rangle$ (lower right) for the d+Au centrality integrated (open circles) and p+p (closed circles) $\pi^0 - h^{\pm}$ correlations for a constant associated hadron p_T from 2.5-5 GeV.

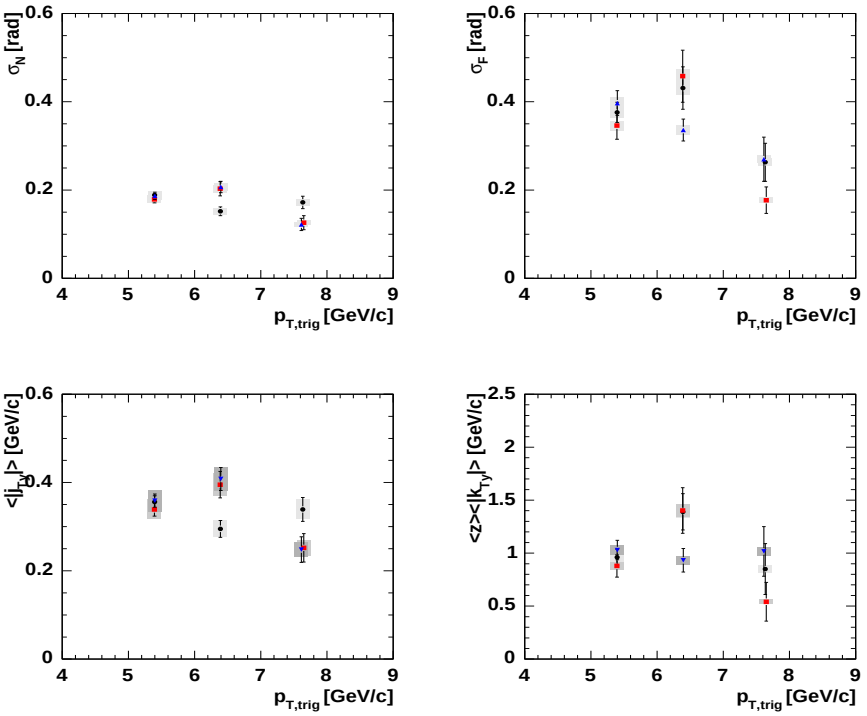

Figure 12: The extracted near angle width (upper left), far angle width (upper right), $\langle |j_{\perp y}| \rangle$(lower left), and $\langle z \rangle \langle |k_{\perp y}| \rangle$ (lower right) for the d+Au centrality binned $\pi^0 - h^{\pm}$ correlations for a constant associated hadron p_T from 2.5-5 GeV. The black circles are 0-20%, red squares are 20-40%, blue triangles are 40-88%

3.2.3 Constant π^0 Trigger in d+Au and p+p

In this case we have a π^0 trigger of $5-10$ GeV and vary the associated hadrons. The corresponding conditional yield distributions are found in Appendix E. Figures 13 - 16 outline the shape and yield analysis for d+Au and p+p $\pi^0 - h^{\pm}$ correlations with a fixed trigger π^0 p_T.

Figs. 13 and 14 show the jet shape results for the both d+Au centrality integrated, centrality binned, and p+p. There is no difference between d+Au and p+p and no obvious trend in centrality. Figs. 15 and 16 show the jet conditional yield results for d+Au centrality integrated, centrality binned, and p+p. Again, within errors, there is no difference between d+Au and p+p and no obvious centrality dependence to the yields.

To quantify the difference in the x_E distributions we fit an exponential function to the data. Table **??** outlines the results of the fit to the data.

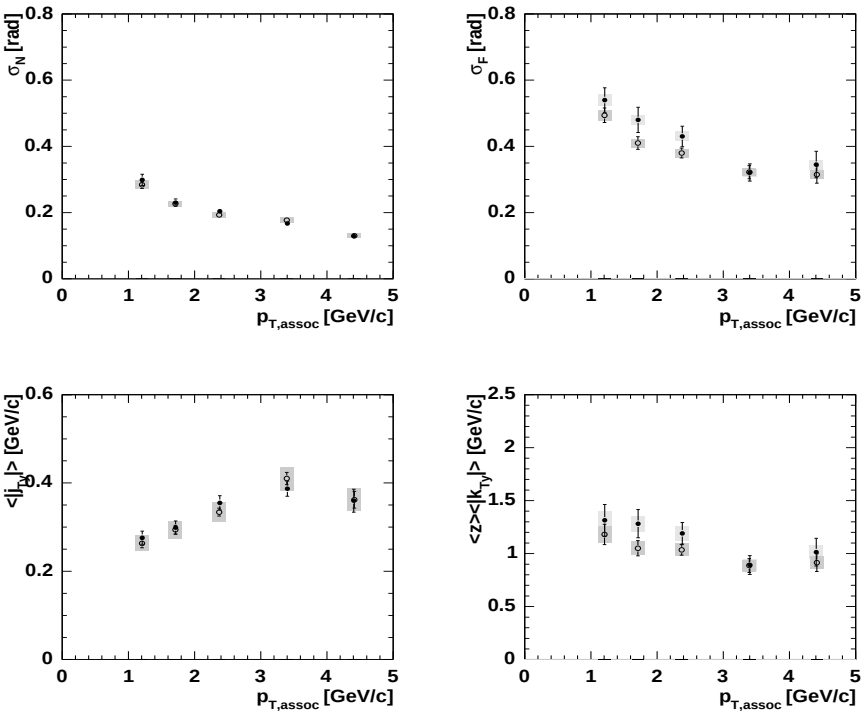

Figure 13: The extracted near angle width (upper left), far angle width (upper right), $\langle|j_{\perp y}|\rangle$ (lower left), and $\langle z\rangle\langle|k_{\perp y}|\rangle$ (lower right) for the d+Au centrality integrated and p+p $\pi^0 - h^{\pm}$ correlations for a constant trigger π^0 p_T 5-10 GeV/c.

Bin/Species	M	slope	χ^2/NDF
p+p	17.7 ± 1.6	6.66 ± 0.22	16.7/3
d+Au CentInt	20.1 ± 1.3	6.72 ± 0.12	66.9/3
d+Au 0-20%	26.1 ± 2.7	7.44 ± 0.27	27.0/3
d+Au 20-40%	24.2 ± 2.8	7.34 ± 0.29	18.3/3
d+Au 40-88%	12.1 ± 1.2	5.32 ± 0.25	54.0/3

Table 2: Fit results for the function $\frac{dN}{dx_E} = Mexp(-slope \times x_E)$.

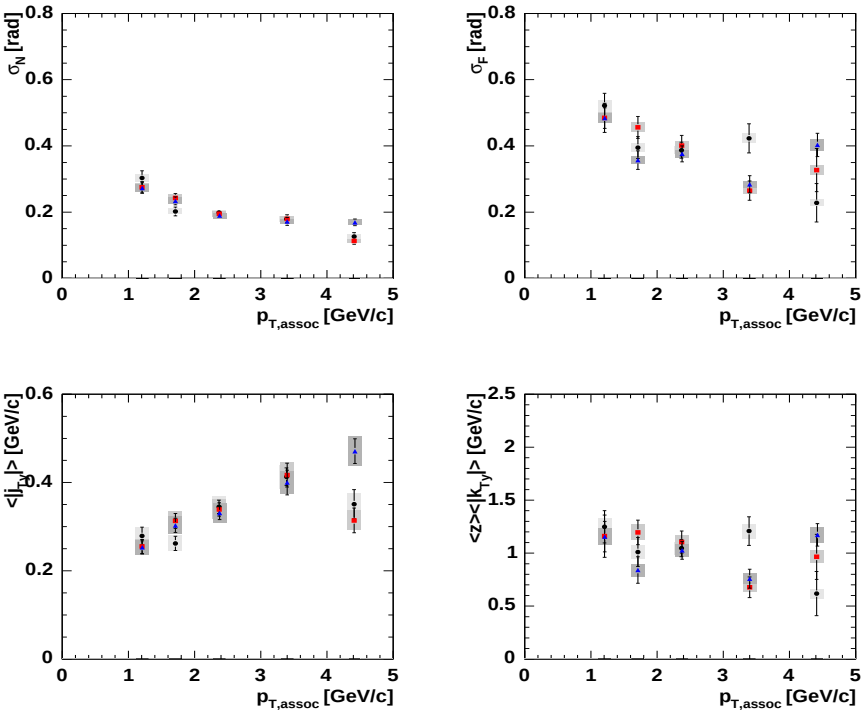

Figure 14: The extracted near angle width (upper left), far angle width (upper right), $\langle|j_{\perp y}|\rangle$ (lower left), and $\langle z\rangle\langle|k_{\perp y}|\rangle$ (lower right) for the d+Au centrality binned $\pi^0 - h^{\pm}$ correlations for a constant trigger π^0 p_T 5-10 GeV/c. The black circles are 0-20%, red squares are 20-40%, blue triangles are 40-88%

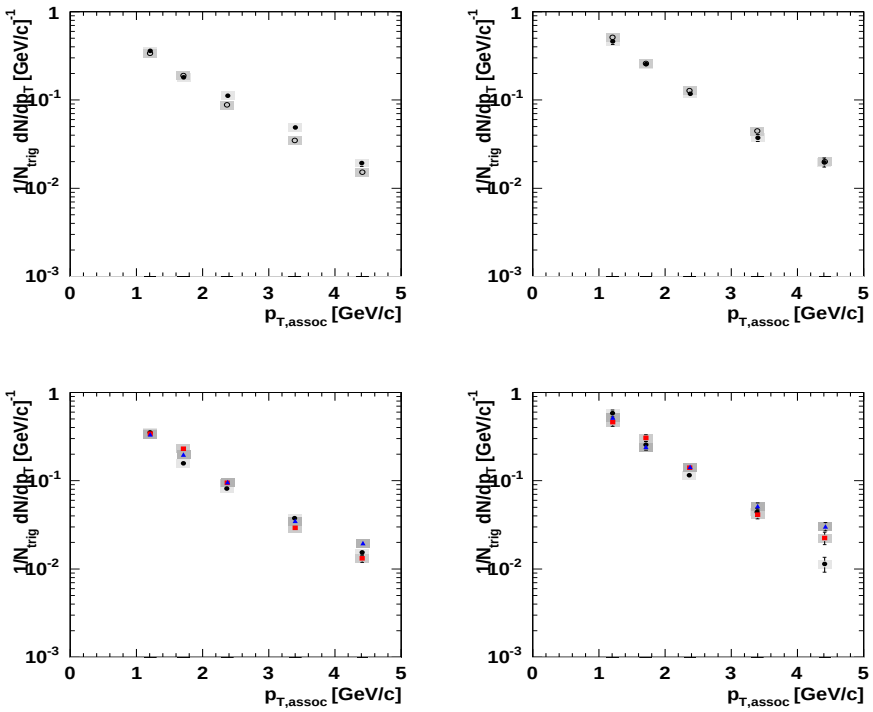

Figure 15: Extracted conditional yields as a function of p_T. Upper plots are centrality integrated d+Au (open circles) and p+p (closed circles). The lower plots are centrality binned d+Au data: black circles 0-20%, red squares 20-40%, and blue triangles 40-88%. The left hand plots are near yield; right hand plots are far yield.

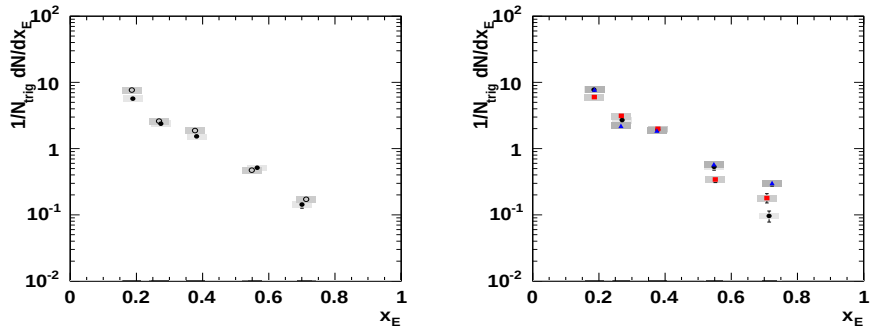

Figure 16: Extracted far yield vs. x_E. Left hand plot centrality integrated d+Au (open circles) and p+p (closed circles). Right hand plot is a function of centrality: black circles 0-20%, red squares 20-40%, and blue triangles 40-88%.

A List of Excluded Runs for the d+Au dataset

The following runs were Photon Converter Runs and excluded from this analysis

```
75365 75377 75379 75399 75401 75403 75532 75533 75547 75549 75550
75587 75619 75622 75631 75636 75747 75794 75795 75796 75800 75983
75994 76050 76053 76070 76274 76276 76284
```

The following runs were excluded because of large deviations from $\langle p_T \rangle$ in either the East of West arm

```
67780 67782 67786 67788 68037 68045 69489 69721 69722 69723 69724
69725 69726 69749 69750 69751 69752 69762 69841
```

The following runs were excluded because of large deviations from $\langle n \rangle_{East} - \langle n \rangle_{West}$

```
67781 67786 69489 69723 69726 69752 69841 70257
```

The following runs were excluded because the ERT trigger was unstable

```
Runs < 71344
```

Based on the mean photon multiplicity and the mean photon p_T in the EmCal, no runs were excluded from the analysis. This applies only to those runs that pass the ERT QA.

There is some overlap in the last two sets of excluded runs. This is mostly due to low statistics in certain runs.

B $h^{\pm} - h^{\pm}$ Conditional Yield Distributions and Table of Values

The following are the fixed-p_T $h^{\pm} - h^{\pm}$ conditional yield distributions from where we derive all quantities.

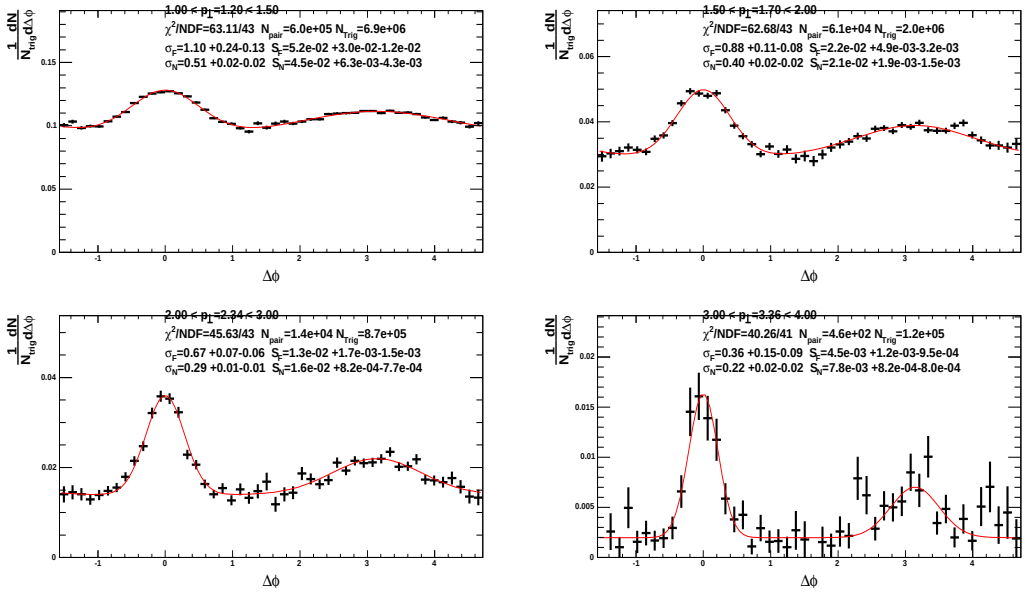

Figure 17: MinBias fixed-p_T $h^{\pm} - h^{\pm}$ Conditional Yield Distributions

$\langle p_T \rangle$ (GeV/c^2)	$\sigma_N(rad)$	$\sigma_F(rad)$	$\langle \lvert j_{\perp y} \rvert \rangle$ (GeV/c^2)	$\langle \lvert k_{\perp y} \rvert \rangle$ (GeV/c^2)
1.20	$0.5126^{+0.0248+0.0000}_{-0.0212-0.0130}$	$1.1022^{+0.2397+0.0000}_{-0.1341-0.0600}$	$0.3279^{+0.0154+0.0143}_{-0.0132-0.0166}$	$1.9118^{+0.4523+1.3764}_{-0.2544-1.3765}$
1.70	$0.3980^{+0.0213+0.0010}_{-0.0188-0.0188}$	$0.8793^{+0.1104+0.0000}_{-0.0830-0.0461}$	$0.3690^{+0.0194+0.0096}_{-0.0172-0.0200}$	$0.9229^{+0.1259+0.2438}_{-0.0949-0.2470}$
2.34	$0.2884^{+0.0136+0.0047}_{-0.0129-0.0139}$	$0.6659^{+0.0657+0.0142}_{-0.0577-0.0441}$	$0.3744^{+0.0175+0.0077}_{-0.0166-0.0186}$	$0.6837^{+0.0765+0.0718}_{-0.0672-0.1092}$
3.36	$0.2159^{+0.0211+0.0067}_{-0.0195-0.0000}$	$0.3587^{+0.1519+0.4028}_{-0.0921-0.0880}$	$0.4053^{+0.0393+0.0129}_{-0.0364-0.0029}$	$0.5499^{+0.3296+1.2636}_{-0.2000-0.2762}$

Table 3: Table of jet shape values for the fixed-p_T $h^{\pm} - h^{\pm}$ MinBias d+Au results.

$\langle p_T \rangle$ (GeV/c^2)	x_E	$dN_{near}/dp_T(GeV/c)^{-1}$	$dN_{far}/dp_T(GeV/c)^{-1}$	dN_{near}/dx_E	dN_{far}/dx_E
1.20	0.7097	$0.1893^{+0.0127+0.0337}_{-0.0086-0.0277}$	$0.2074^{+0.0597+0.0369}_{-0.0244-0.0393}$	$0.2868^{+0.0192+0.0511}_{-0.0130-0.0420}$	$0.3143^{+0.0905+0.0559}_{-0.0370-0.0596}$
1.70	0.7686	$0.0731^{+0.0037+0.0127}_{-0.0029-0.0107}$	$0.0861^{+0.0098+0.0149}_{-0.0064-0.0125}$	$0.1463^{+0.0075+0.0253}_{-0.0058-0.0214}$	$0.1722^{+0.0196+0.0298}_{-0.0129-0.0250}$
2.34	0.8085	$0.0237^{+0.0008+0.0045}_{-0.0008-0.0033}$	$0.0268^{+0.0017+0.0050}_{-0.0015-0.0048}$	$0.0717^{+0.0025+0.0136}_{-0.0023-0.0101}$	$0.0813^{+0.0051+0.0151}_{-0.0044-0.0146}$
3.36	0.8672	$0.0103^{+0.0008+0.0023}_{-0.0008-0.0017}$	$0.0090^{+0.0012+0.0084}_{-0.0009-0.0016}$	$0.0412^{+0.0033+0.0091}_{-0.0032-0.0067}$	$0.0362^{+0.0049+0.0334}_{-0.0038-0.0063}$

Table 4: Table of jet yield values for the fixed-p_T $h^{\pm} - h^{\pm}$ MinBias d+Au results.

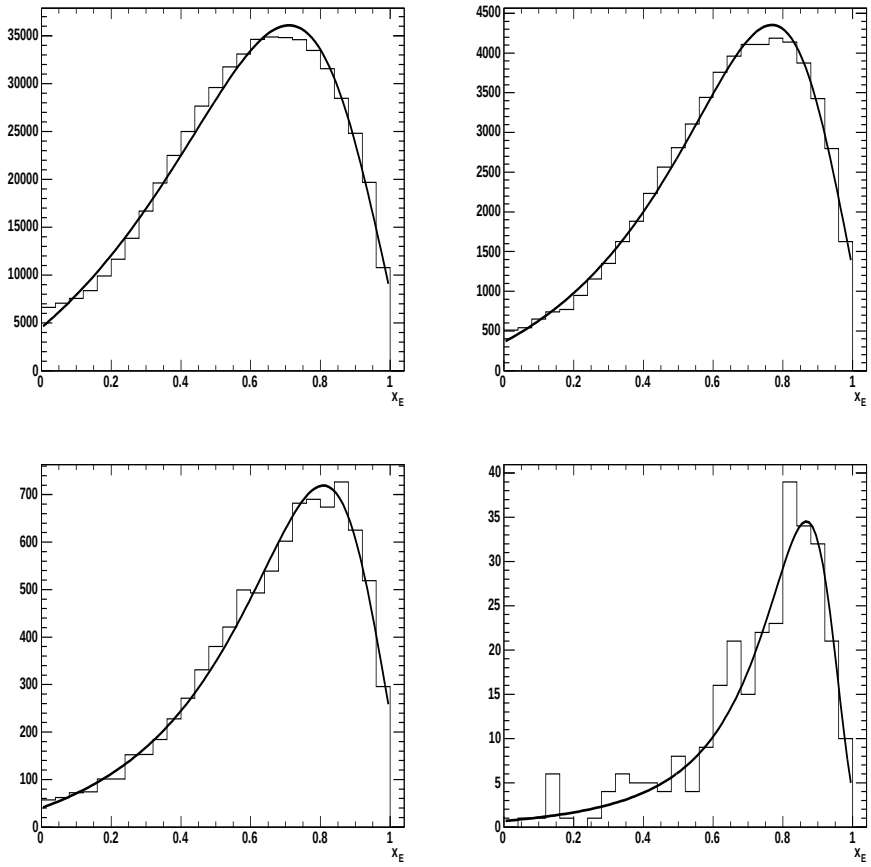

Figure 18: MinBias fixed-p_T $h^{\pm} - h^{\pm}$ x_E distributions.

C $\pi^0 - h^{\pm}$ Conditional Yield Distributions for Fixed Associated Hadron p_T

The following are the assorted-p_T $\pi^0 - h^{\pm}$ conditional yield distributions for a fixed associated hadron p_T of $2 - 5GeV$

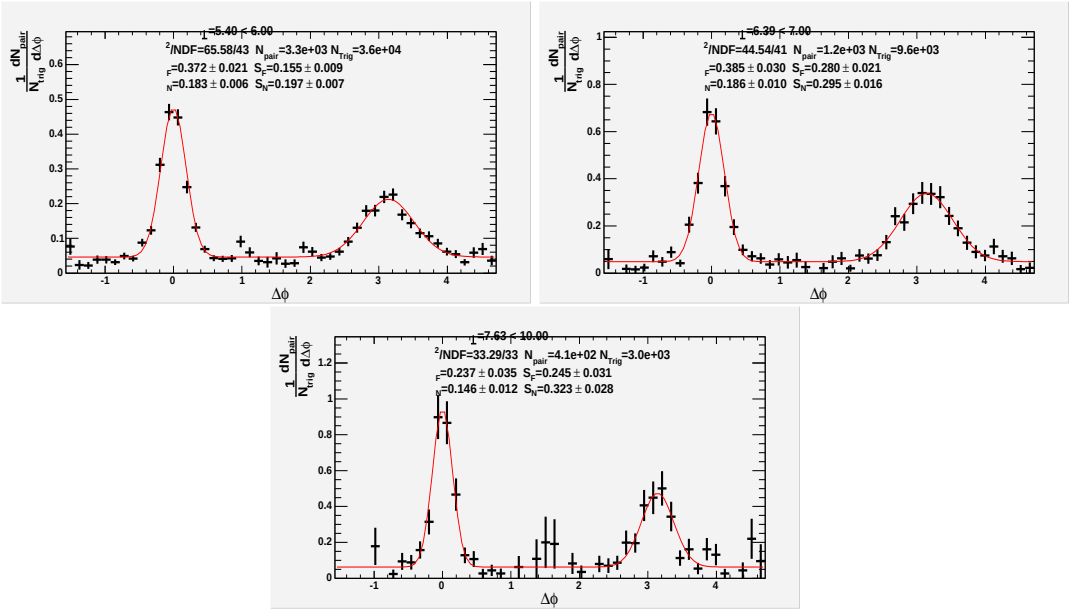

Figure 19: $\pi^0 - h^{\pm}$ centrality integrated conditional yield distributions for a constant hadron p_T of 2-5 GeV/c. The fit is given by Equation 5. A table of extracted widths is given in Table 5.

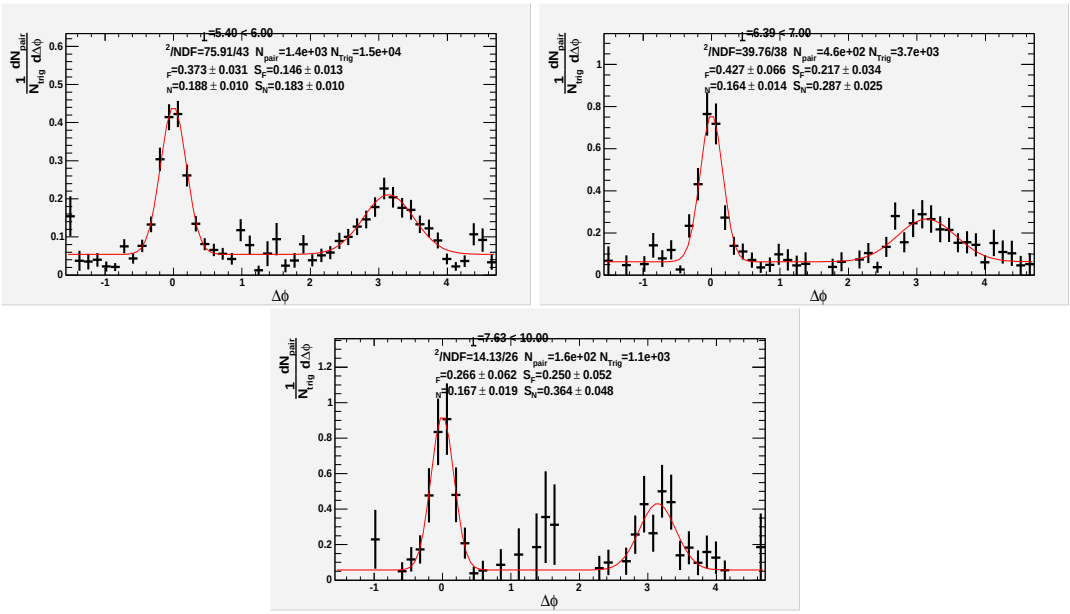

Figure 20: 0-20% central $\pi^0 - h^{\pm}$ conditional yield distributions. The fit is given by Equation 5. A table of extracted widths is given in Table 6.

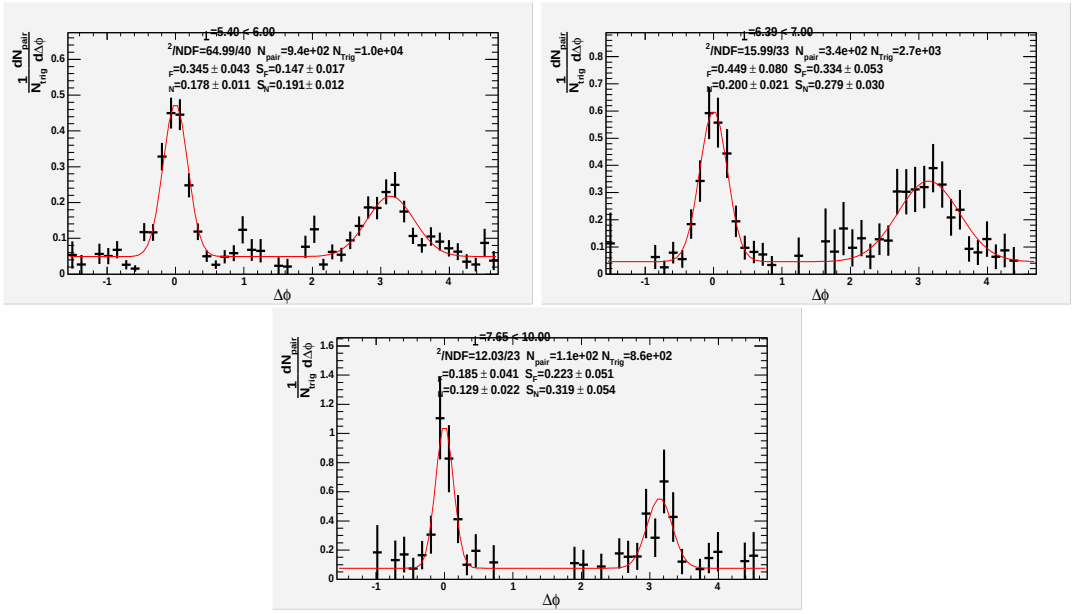

Figure 21: 20-40% central $\pi^0 - h^{\pm}$ conditional yield distributions. The fit is given by Equation 5. A table of extracted widths is given in Table 7.

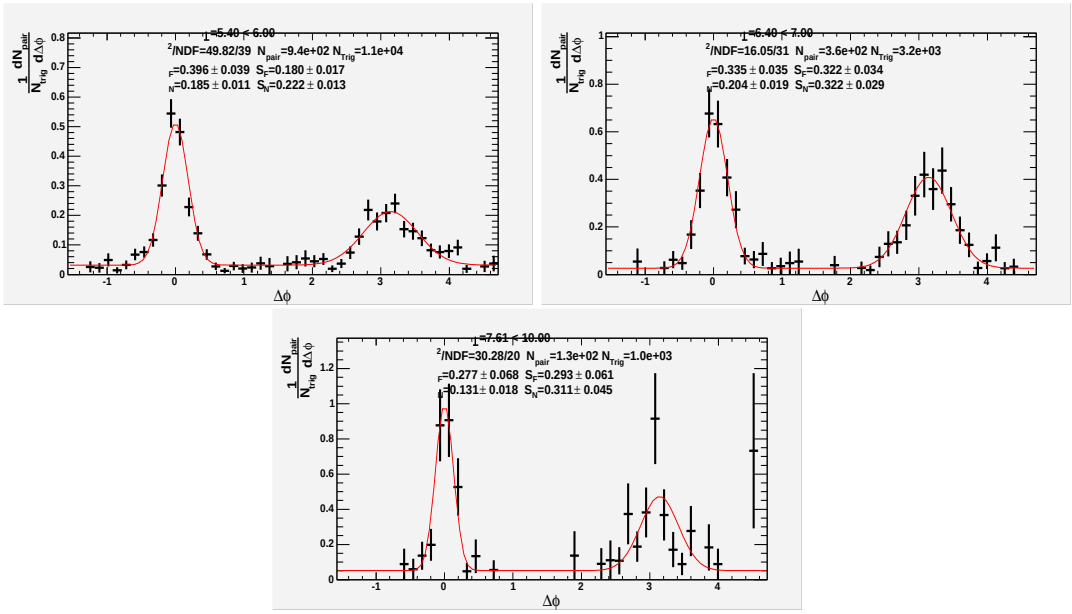

Figure 22: 40-88% central $\pi^0 - h^{\pm}$ conditional yield distributions. The fit is given by Equation 5. A table of extracted widths is given in Table 8.

D Tables of Values for Jet Shapes and Yields for d+Au $\pi^0 - h^\pm$ Correlations with Fixed Associated Hadron

$p_{T,trig}$	$\sigma_N(rad)$	$\sigma_F(rad)$	$\langle\|j_{Ty}\|\rangle$	$\langle z\rangle\langle\|k_{Ty}\|\rangle$
5.398	$0.184 \pm 0.004 \pm 0.008$	$0.374 \pm 0.015 \pm 0.012$	$0.348 \pm 0.008 \pm 0.023$	$0.961 \pm 0.050 \pm 0.040$
6.391	$0.188 \pm 0.007 \pm 0.008$	$0.388 \pm 0.022 \pm 0.012$	$0.366 \pm 0.014 \pm 0.024$	$1.181 \pm 0.084 \pm 0.048$
7.631	$0.147 \pm 0.009 \pm 0.006$	$0.233 \pm 0.025 \pm 0.007$	$0.293 \pm 0.018 \pm 0.019$	$0.773 \pm 0.138 \pm 0.031$

Table 5: Near and Far angle widths extracted from centrality integrated d+Au $\pi^0 - h^\pm$ correlations with a constant hadron p_T of 2-5 GeV/c ($\langle p_{T,assoc}\rangle = 2.659$ GeV/c).

$p_{T,trig}$	$\sigma_N(rad)$	$\sigma_F(rad)$	$\langle\|j_{Ty}\|\rangle$	$\langle z\rangle\langle\|k_{Ty}\|\rangle$
5.398	$0.189 \pm 0.007 \pm 0.008$	$0.376 \pm 0.023 \pm 0.012$	$0.356 \pm 0.014 \pm 0.023$	$0.960 \pm 0.076 \pm 0.040$
6.390	$0.152 \pm 0.010 \pm 0.007$	$0.431 \pm 0.048 \pm 0.014$	$0.295 \pm 0.019 \pm 0.019$	$1.390 \pm 0.172 \pm 0.056$
7.634	$0.172 \pm 0.014 \pm 0.007$	$0.263 \pm 0.043 \pm 0.008$	$0.339 \pm 0.027 \pm 0.022$	$0.850 \pm 0.240 \pm 0.034$

Table 6: Near and Far angle widths extracted from 0-20% central d+Au $\pi^0 - h^\pm$ correlations with a constant hadron p_T of 2-5 GeV/c. ($\langle p_{T,assoc}\rangle = 2.636$ GeV/c)

$p_{T,trig}$	$\sigma_N(rad)$	$\sigma_F(rad)$	$\langle\|j_{Ty}\|\rangle$	$\langle z\rangle\langle\|k_{Ty}\|\rangle$
5.395	$0.179 \pm 0.008 \pm 0.008$	$0.346 \pm 0.031 \pm 0.011$	$0.339 \pm 0.015 \pm 0.022$	$0.879 \pm 0.105 \pm 0.036$
6.387	$0.203 \pm 0.016 \pm 0.009$	$0.458 \pm 0.059 \pm 0.015$	$0.395 \pm 0.030 \pm 0.026$	$1.402 \pm 0.215 \pm 0.057$
7.650	$0.126 \pm 0.016 \pm 0.005$	$0.177 \pm 0.030 \pm 0.006$	$0.252 \pm 0.032 \pm 0.017$	$0.541 \pm 0.183 \pm 0.022$

Table 7: Near and Far angle widths extracted from 20-40% central d+Au $\pi^0 - h^\pm$ correlations with a constant hadron p_T of 2-5 ($\langle p_{T,assoc}\rangle = 2.666$ GeV/c) GeV/c.

$p_{T,trig}$	$\sigma_N(rad)$	$\sigma_F(rad)$	$\langle\|j_{Ty}\|\rangle$	$\langle z\rangle\langle\|k_{Ty}\|\rangle$
5.399	$0.187 \pm 0.008 \pm 0.008$	$0.397 \pm 0.028 \pm 0.013$	$0.359 \pm 0.015 \pm 0.024$	$1.029 \pm 0.092 \pm 0.043$
6.396	$0.207 \pm 0.013 \pm 0.009$	$0.336 \pm 0.025 \pm 0.011$	$0.408 \pm 0.026 \pm 0.027$	$0.932 \pm 0.111 \pm 0.038$
7.613	$0.122 \pm 0.014 \pm 0.005$	$0.270 \pm 0.050 \pm 0.009$	$0.248 \pm 0.029 \pm 0.016$	$1.016 \pm 0.235 \pm 0.041$

Table 8: Near and Far angle widths extracted from 40-88% central d+Au $\pi^0 - h^\pm$ correlations with a constant hadron p_T of 2-5 GeV/c. ($\langle p_{T,assoc}\rangle = 2.707$ GeV/c)

E $\pi^0 - h^{\pm}$ Conditional Yield Distributions for Fixed Trigger π^0 p_T

The following are the assorted-p_T $\pi^0 - h^{\pm}$ conditional yield distributions for a fixed trigger p_T of 5-10 GeV/c

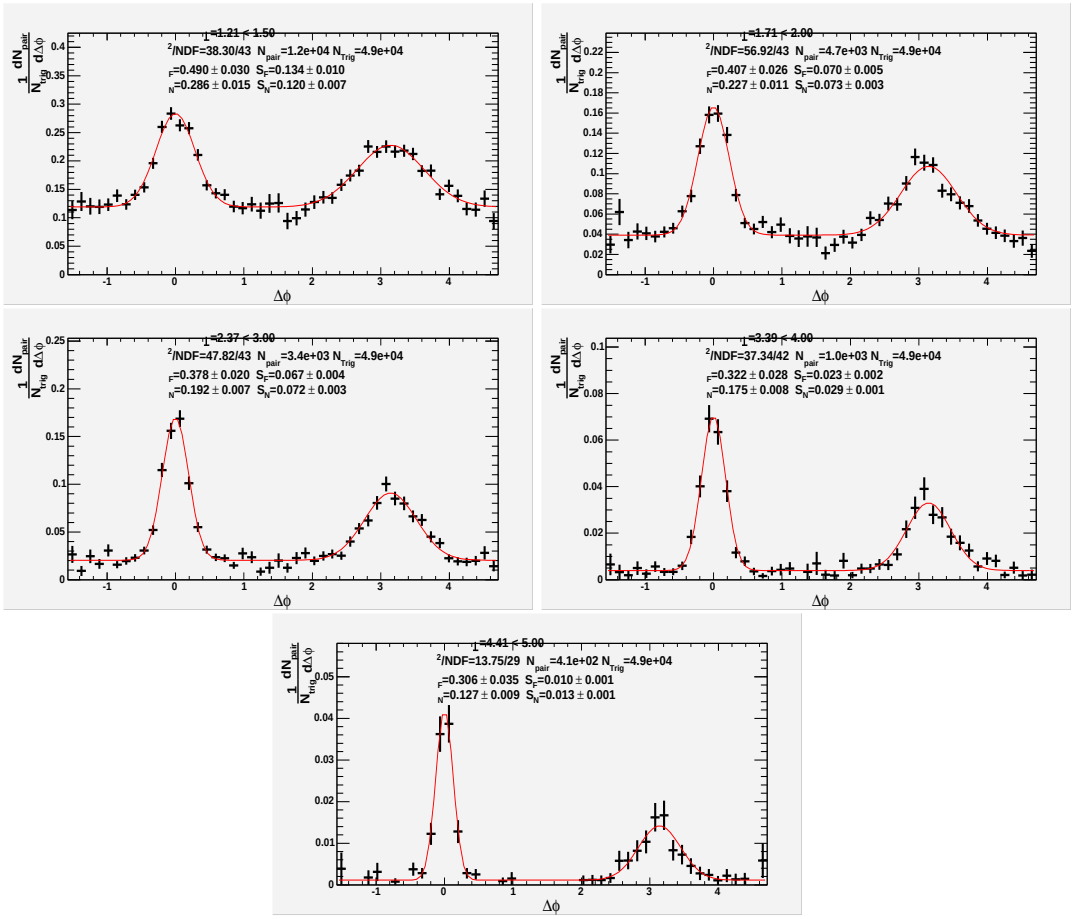

Figure 23: Constant π^0 trigger $\pi^0 - h^{\pm}$ d+Au centrality integrated conditional yield distributions. The fit is given by Equation 5. Shape and yield results are given in Tables 9 and 10

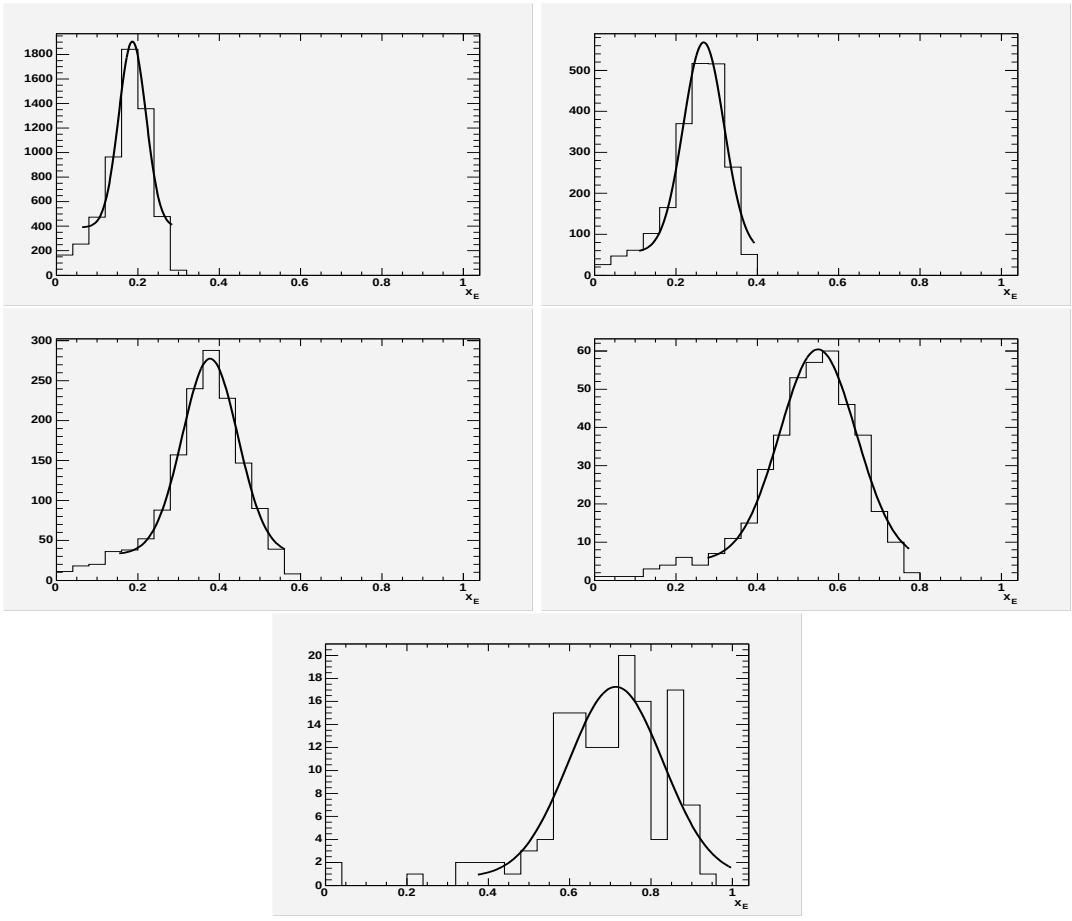

Figure 24: Constant π^0 trigger $\pi^0 - h^{\pm}$ d+Au centrality integrated x_E distributions. The fit is a gaussian plus a flat term. x_E results are given in Table 10.

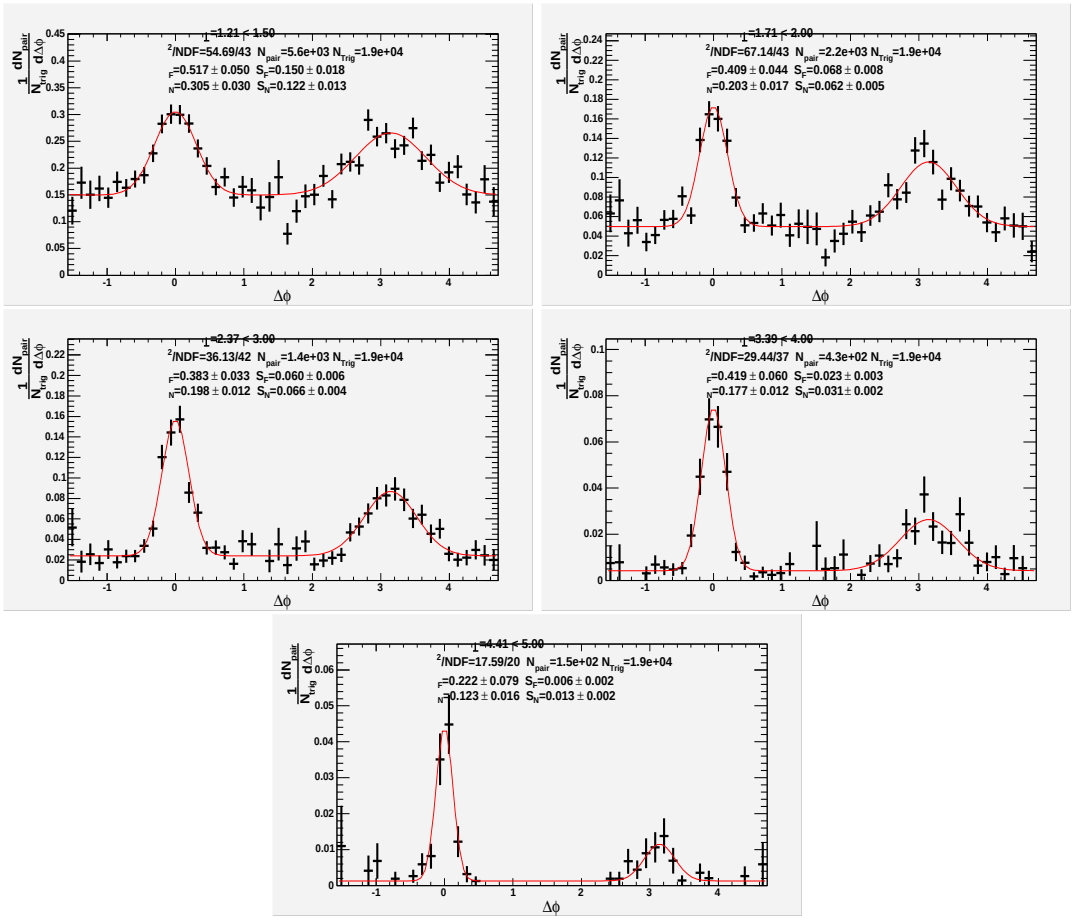

Figure 25: Constant π^0 trigger $\pi^0 - h^{\pm}$ conditional d+Au 0-20% central conditional yield distributions. The fit is given by Equation 5. Shape and yield results are given in Tables 11 and 12

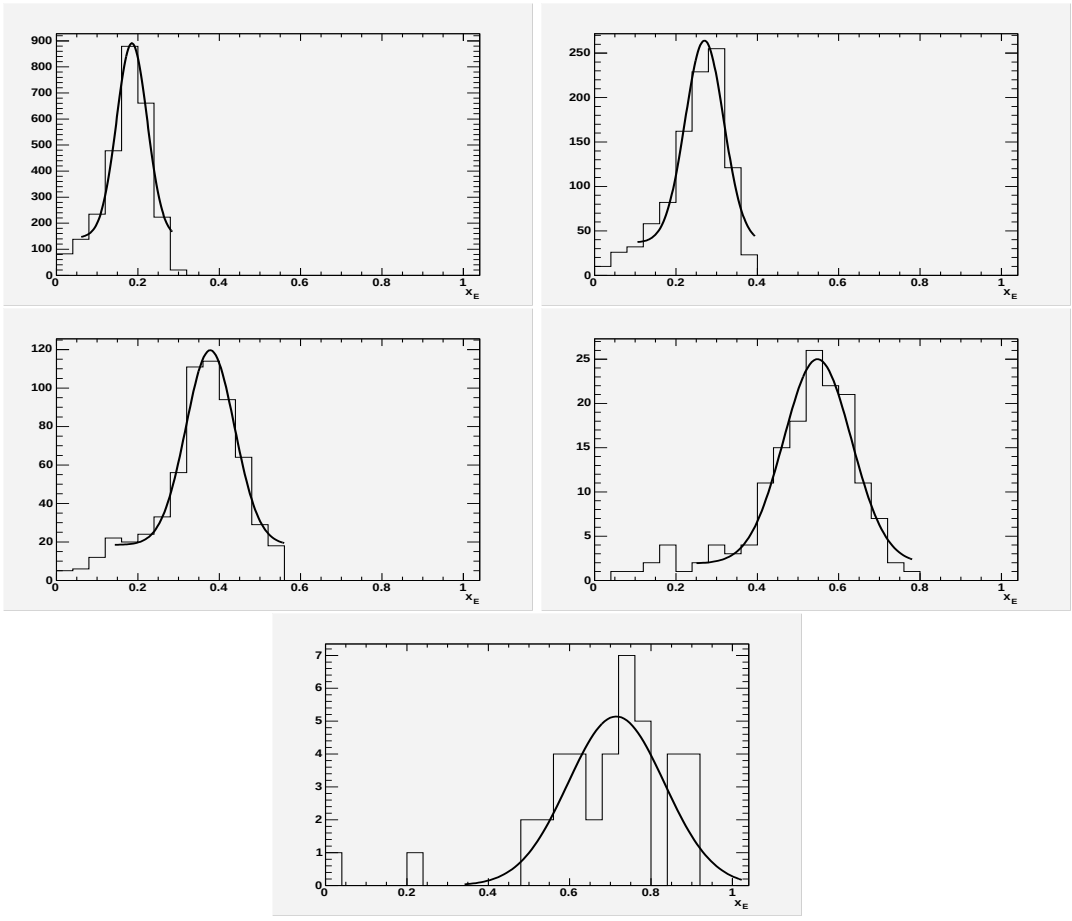

Figure 26: Constant π^0 trigger $\pi^0 - h^{\pm}$ d+Au 0-20% x_E distributions. The fit is a gaussian plus a flat term. x_E results are given in Table 12.

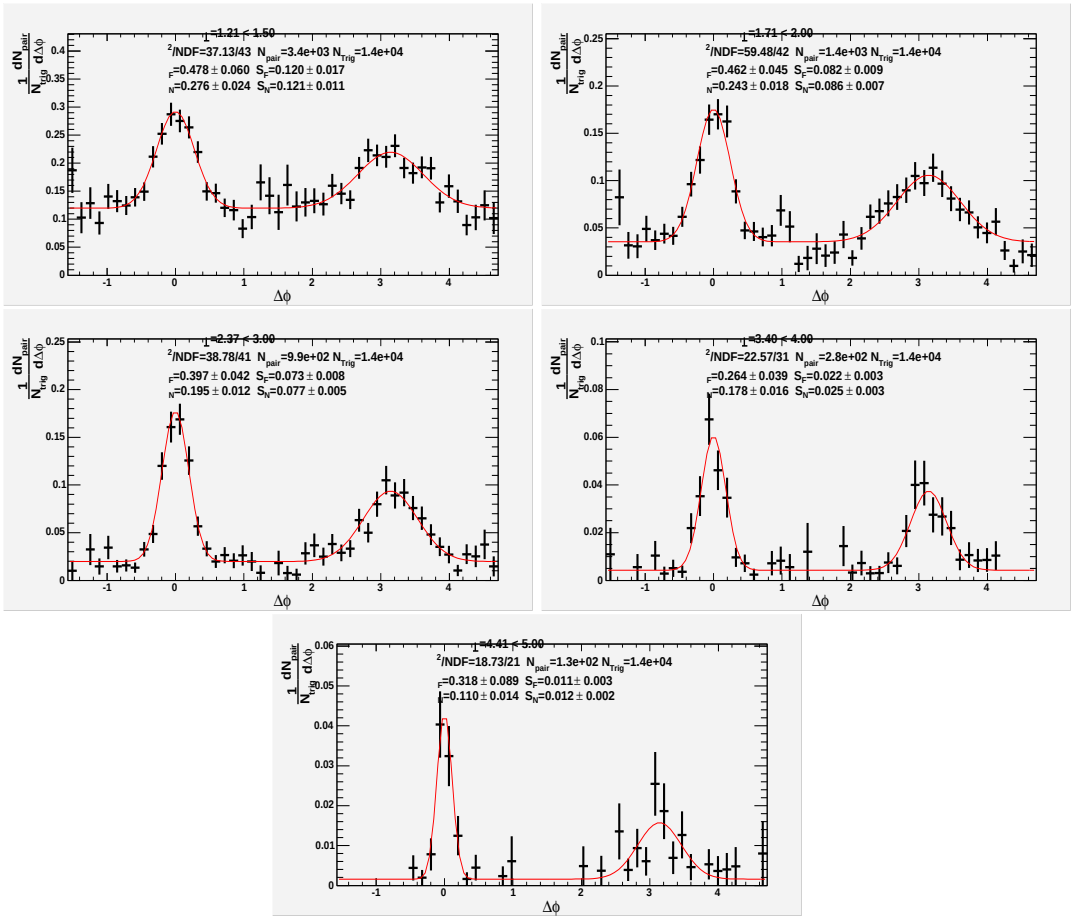

Figure 27: Constant π^0 trigger $\pi^0 - h^{\pm}$ conditional d+Au 20-40% central conditional yield distributions. The fit is given by Equation 5. Shape and yield results are given in Tables 13 and 14.

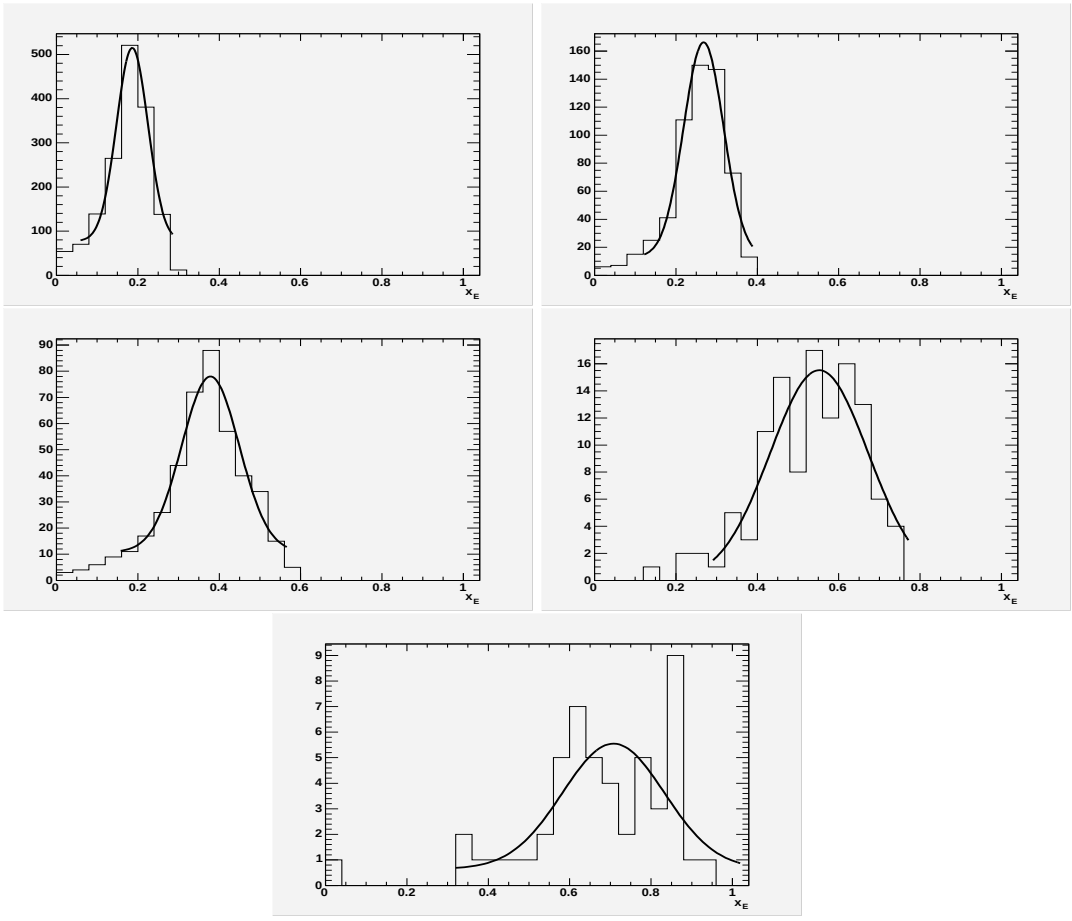

Figure 28: Constant π^0 trigger $\pi^0 - h^{\pm}$ d+Au 20-40% x_E distributions. The fit is a gaussian plus a flat term. x_E results are given in Table 14.

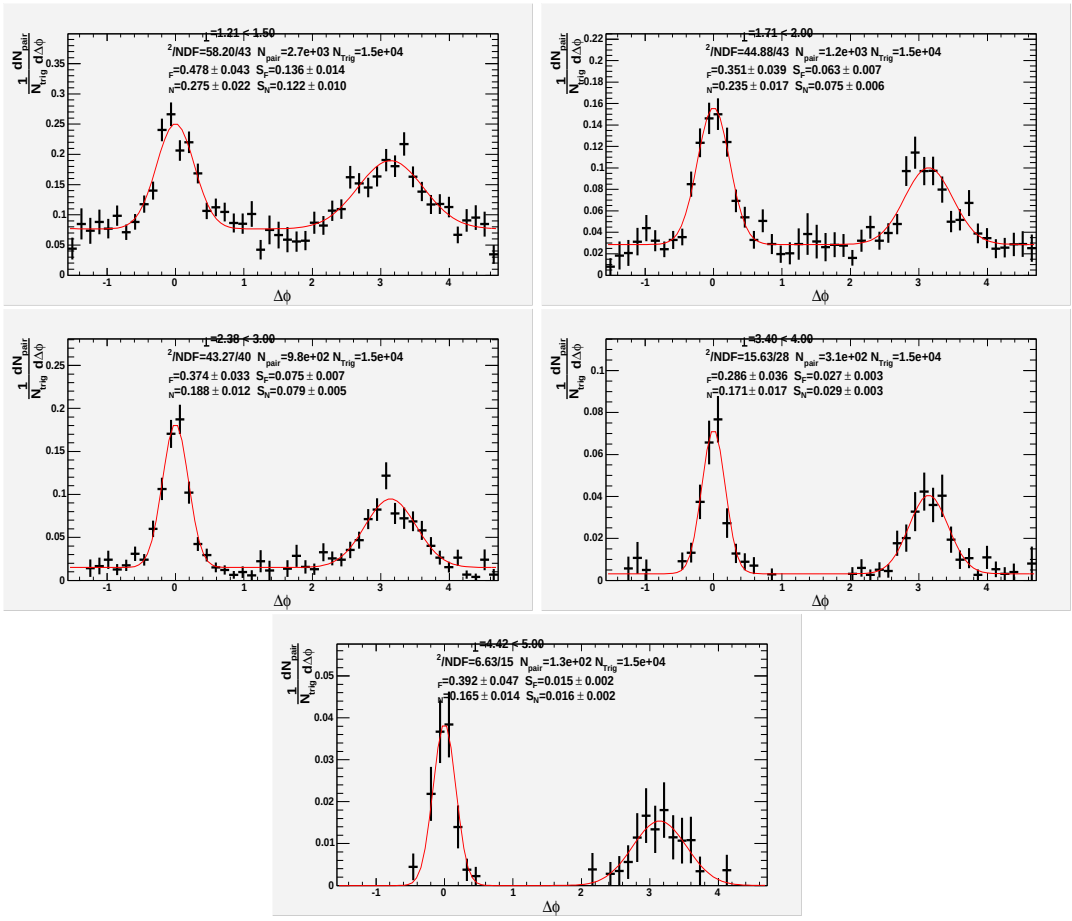

Figure 29: Constant π^0 trigger $\pi^0 - h^{\pm}$ conditional d+Au 40-88% central conditional yield distributions. The fit is given by Equation 5. Shape and yield results are given in Tables 15 and 16.

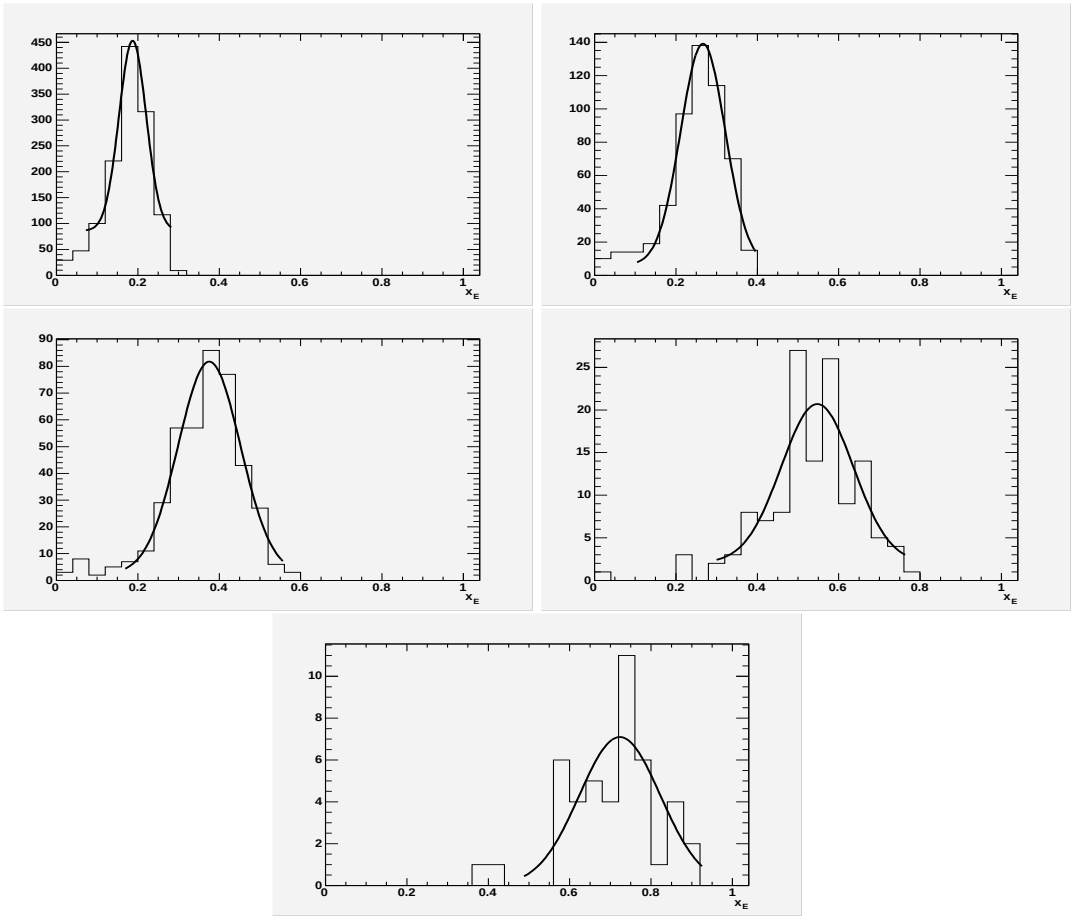

Figure 30: Constant π^0 trigger $\pi^0 - h^{\pm}$ d+Au 40-88% x_E distributions. The fit is a gaussian plus a flat term. x_E results are given in Table 16.

F Tables of Values for Jet Shapes and Yields for d+Au $\pi^0 - h^\pm$ Correlations with Fixed Trigger π^0

$p_{T,assoc}$	$\sigma_N(rad)$	$\sigma_F(rad)$	$\langle\|j_{Ty}\|\rangle$	$\langle z\rangle\langle\|k_{Ty}\|\rangle$
1.208	$0.284 \pm 0.011 \pm 0.012$	$0.494 \pm 0.022 \pm 0.016$	$0.263 \pm 0.010 \pm 0.018$	$1.181 \pm 0.096 \pm 0.078$
1.711	$0.227 \pm 0.007 \pm 0.009$	$0.410 \pm 0.019 \pm 0.013$	$0.294 \pm 0.010 \pm 0.020$	$1.050 \pm 0.072 \pm 0.065$
2.371	$0.193 \pm 0.005 \pm 0.008$	$0.380 \pm 0.015 \pm 0.012$	$0.334 \pm 0.009 \pm 0.022$	$1.035 \pm 0.050 \pm 0.060$
3.394	$0.177 \pm 0.006 \pm 0.008$	$0.322 \pm 0.020 \pm 0.012$	$0.410 \pm 0.014 \pm 0.027$	$0.887 \pm 0.066 \pm 0.055$
4.414	$0.130 \pm 0.007 \pm 0.007$	$0.315 \pm 0.026 \pm 0.013$	$0.362 \pm 0.019 \pm 0.026$	$0.915 \pm 0.084 \pm 0.058$

Table 9: Near and Far angle widths extracted from centrality integrated d+Au $\pi^0 - h^\pm$ correlations with a constant π^0 p_T of 5-10 GeV/c. ($\langle p_{T,trig}\rangle = 5.729$ GeV/c)

$p_{T,assoc}$	x_E	dN_{near}/dp_T	dN_{far}/dp_T	dN_{near}/dx_E	dN_{far}/dx_E
1.208	0.187 ± 0.033	$0.338 \pm 0.013 \pm 0.035$	$0.513 \pm 0.027 \pm 0.060$	$1.934 \pm 0.077 \pm 0.203$	$7.683 \pm 0.405 \pm 0.899$
1.711	0.268 ± 0.050	$0.190 \pm 0.006 \pm 0.020$	$0.259 \pm 0.013 \pm 0.028$	$1.086 \pm 0.035 \pm 0.114$	$2.603 \pm 0.134 \pm 0.279$
2.371	0.378 ± 0.068	$0.088 \pm 0.002 \pm 0.009$	$0.128 \pm 0.005 \pm 0.013$	$0.505 \pm 0.013 \pm 0.053$	$1.878 \pm 0.076 \pm 0.197$
3.394	0.549 ± 0.094	$0.035 \pm 0.001 \pm 0.004$	$0.044 \pm 0.003 \pm 0.005$	$0.199 \pm 0.007 \pm 0.021$	$0.473 \pm 0.028 \pm 0.050$
4.414	0.713 ± 0.116	$0.015 \pm 0.001 \pm 0.002$	$0.020 \pm 0.002 \pm 0.002$	$0.087 \pm 0.004 \pm 0.009$	$0.172 \pm 0.014 \pm 0.018$

Table 10: Near and Far yield and x_E distirbutions extracted from centrality integrated d+Au $\pi^0 - h^\pm$ correlations with a constant π^0 p_T of 5-10 GeV/c. ($\langle p_{T,trig}\rangle = 5.729$ GeV/c)

$p_{T,assoc}$	$\sigma_N(rad)$	$\sigma_F(rad)$	$\langle\|j_{Ty}\|\rangle$	$\langle z\rangle\langle\|k_{Ty}\|\rangle$
1.207	$0.303 \pm 0.022 \pm 0.012$	$0.522 \pm 0.037 \pm 0.017$	$0.279 \pm 0.020 \pm 0.019$	$1.248 \pm 0.152 \pm 0.082$
1.711	$0.202 \pm 0.013 \pm 0.008$	$0.395 \pm 0.033 \pm 0.013$	$0.262 \pm 0.016 \pm 0.018$	$1.011 \pm 0.136 \pm 0.063$
2.368	$0.199 \pm 0.009 \pm 0.009$	$0.387 \pm 0.024 \pm 0.012$	$0.345 \pm 0.015 \pm 0.023$	$1.047 \pm 0.082 \pm 0.061$
3.389	$0.179 \pm 0.009 \pm 0.008$	$0.423 \pm 0.044 \pm 0.015$	$0.413 \pm 0.020 \pm 0.027$	$1.208 \pm 0.135 \pm 0.070$
4.410	$0.126 \pm 0.012 \pm 0.006$	$0.228 \pm 0.058 \pm 0.010$	$0.351 \pm 0.033 \pm 0.025$	$0.618 \pm 0.209 \pm 0.044$

Table 11: Near and Far angle widths extracted from 0-20% central d+Au $\pi^0 - h^\pm$ correlations with a constant π^0 p_T of 5-10 GeV/c. ($\langle p_{T,trig}\rangle = 5.717$ GeV/c)

$p_{T,assoc}$	x_E	dN_{near}/dp_T	dN_{far}/dp_T	dN_{near}/dx_E	dN_{far}/dx_E
1.207	0.185 ± 0.037	$0.352 \pm 0.027 \pm 0.037$	$0.582 \pm 0.051 \pm 0.068$	$2.011 \pm 0.154 \pm 0.211$	$7.761 \pm 0.687 \pm 0.908$
1.711	0.270 ± 0.047	$0.158 \pm 0.009 \pm 0.017$	$0.256 \pm 0.023 \pm 0.027$	$0.901 \pm 0.053 \pm 0.095$	$2.704 \pm 0.238 \pm 0.289$
2.368	0.378 ± 0.060	$0.082 \pm 0.004 \pm 0.009$	$0.116 \pm 0.008 \pm 0.012$	$0.467 \pm 0.021 \pm 0.049$	$1.936 \pm 0.134 \pm 0.203$
3.389	0.548 ± 0.083	$0.038 \pm 0.002 \pm 0.004$	$0.044 \pm 0.005 \pm 0.005$	$0.215 \pm 0.012 \pm 0.023$	$0.530 \pm 0.057 \pm 0.056$
4.410	0.715 ± 0.118	$0.015 \pm 0.001 \pm 0.002$	$0.011 \pm 0.002 \pm 0.001$	$0.088 \pm 0.007 \pm 0.009$	$0.096 \pm 0.018 \pm 0.010$

Table 12: Near and Far angle yields and x_E distributions extracted from 0-20% central d+Au $\pi^0 - h^\pm$ correlations with a constant π^0 p_T of 5-10 GeV/c. ($\langle p_{T,trig}\rangle = 5.717$ GeV/c)

$p_{T,assoc}$	$\sigma_N(rad)$	$\sigma_F(rad)$	$\langle\|j_{Ty}\|\rangle$	$\langle z\rangle\langle\|k_{Ty}\|\rangle$
1.208	$0.275 \pm 0.017 \pm 0.011$	$0.485 \pm 0.044 \pm 0.016$	$0.255 \pm 0.016 \pm 0.017$	$1.160 \pm 0.199 \pm 0.077$
1.711	$0.243 \pm 0.013 \pm 0.010$	$0.456 \pm 0.033 \pm 0.015$	$0.313 \pm 0.017 \pm 0.021$	$1.195 \pm 0.116 \pm 0.071$
2.372	$0.195 \pm 0.009 \pm 0.008$	$0.401 \pm 0.031 \pm 0.013$	$0.339 \pm 0.015 \pm 0.022$	$1.104 \pm 0.104 \pm 0.063$
3.398	$0.180 \pm 0.012 \pm 0.008$	$0.265 \pm 0.029 \pm 0.010$	$0.417 \pm 0.027 \pm 0.028$	$0.678 \pm 0.098 \pm 0.047$
4.411	$0.113 \pm 0.010 \pm 0.006$	$0.327 \pm 0.065 \pm 0.014$	$0.314 \pm 0.028 \pm 0.022$	$0.965 \pm 0.213 \pm 0.060$

Table 13: Near and Far angle widths extracted from 20-40% central d+Au $\pi^0 - h^{\pm}$ correlations with a constant π^0 p_T of 5-10 GeV/c. ($\langle p_{T,trig}\rangle = 5.728$ GeV/c)

$p_{T,assoc}$	x_E	dN_{near}/dp_T	dN_{far}/dp_T	dN_{near}/dx_E	dN_{far}/dx_E
1.208	0.186 ± 0.038	$0.341 \pm 0.023 \pm 0.036$	$0.462 \pm 0.049 \pm 0.054$	$1.955 \pm 0.132 \pm 0.205$	$6.007 \pm 0.631 \pm 0.703$
1.711	0.268 ± 0.049	$0.230 \pm 0.013 \pm 0.024$	$0.306 \pm 0.027 \pm 0.033$	$1.317 \pm 0.074 \pm 0.138$	$3.121 \pm 0.273 \pm 0.334$
2.372	0.379 ± 0.071	$0.095 \pm 0.004 \pm 0.010$	$0.141 \pm 0.011 \pm 0.015$	$0.542 \pm 0.026 \pm 0.057$	$1.990 \pm 0.151 \pm 0.209$
3.398	0.552 ± 0.120	$0.029 \pm 0.002 \pm 0.003$	$0.041 \pm 0.004 \pm 0.004$	$0.168 \pm 0.013 \pm 0.018$	$0.343 \pm 0.037 \pm 0.036$
4.411	0.708 ± 0.125	$0.013 \pm 0.001 \pm 0.001$	$0.022 \pm 0.004 \pm 0.002$	$0.075 \pm 0.007 \pm 0.008$	$0.180 \pm 0.029 \pm 0.019$

Table 14: Near and Far yields and x_E distributions extracted from 20-40% central d+Au $\pi^0 - h^{\pm}$ correlations with a constant π^0 p_T of 5-10 GeV/c. ($\langle p_{T,trig}\rangle = 5.728$ GeV/c)

$p_{T,assoc}$	$\sigma_N(rad)$	$\sigma_F(rad)$	$\langle\|j_{Ty}\|\rangle$	$\langle z\rangle\langle\|k_{Ty}\|\rangle$
1.208	$0.273 \pm 0.016 \pm 0.011$	$0.484 \pm 0.031 \pm 0.015$	$0.253 \pm 0.015 \pm 0.017$	$1.156 \pm 0.144 \pm 0.077$
1.712	$0.234 \pm 0.012 \pm 0.010$	$0.357 \pm 0.028 \pm 0.011$	$0.303 \pm 0.016 \pm 0.020$	$0.841 \pm 0.125 \pm 0.059$
2.378	$0.190 \pm 0.008 \pm 0.008$	$0.376 \pm 0.024 \pm 0.012$	$0.331 \pm 0.015 \pm 0.022$	$1.027 \pm 0.084 \pm 0.060$
3.399	$0.172 \pm 0.012 \pm 0.007$	$0.284 \pm 0.026 \pm 0.010$	$0.400 \pm 0.028 \pm 0.026$	$0.759 \pm 0.089 \pm 0.049$
4.424	$0.169 \pm 0.010 \pm 0.008$	$0.403 \pm 0.035 \pm 0.017$	$0.471 \pm 0.028 \pm 0.033$	$1.172 \pm 0.106 \pm 0.074$

Table 15: Near and Far angle widths extracted from 40-88% central d+Au $\pi^0 - h^{\pm}$ correlations with a constant π^0 p_T of 5-10 GeV/c. ($\langle p_{T,trig}\rangle = 5.746$ GeV/c)

$p_{T,assoc}$	x_E	dN_{near}/dp_T	dN_{far}/dp_T	dN_{near}/dx_E	dN_{far}/dx_E
1.208	0.187 ± 0.033	$0.335 \pm 0.020 \pm 0.035$	$0.520 \pm 0.040 \pm 0.061$	$1.925 \pm 0.117 \pm 0.202$	$7.790 \pm 0.600 \pm 0.911$
1.712	0.267 ± 0.055	$0.198 \pm 0.011 \pm 0.021$	$0.242 \pm 0.020 \pm 0.026$	$1.138 \pm 0.061 \pm 0.119$	$2.211 \pm 0.183 \pm 0.237$
2.378	0.376 ± 0.076	$0.097 \pm 0.004 \pm 0.010$	$0.144 \pm 0.009 \pm 0.015$	$0.556 \pm 0.025 \pm 0.058$	$1.880 \pm 0.122 \pm 0.197$
3.399	0.547 ± 0.088	$0.035 \pm 0.002 \pm 0.004$	$0.051 \pm 0.005 \pm 0.005$	$0.202 \pm 0.014 \pm 0.021$	$0.583 \pm 0.052 \pm 0.061$
4.424	0.723 ± 0.100	$0.020 \pm 0.002 \pm 0.002$	$0.030 \pm 0.003 \pm 0.003$	$0.113 \pm 0.009 \pm 0.012$	$0.304 \pm 0.032 \pm 0.032$

Table 16: Near and Far yields and x_E distributions extracted from 40-88% central d+Au $\pi^0 - h^{\pm}$ correlations with a constant π^0 p_T of 5-10 GeV/c. ($\langle p_{T,trig}\rangle = 5.746$ GeV/c)

G p+p $\pi^0 - h^{\pm}$ Conditional Yield Distributions

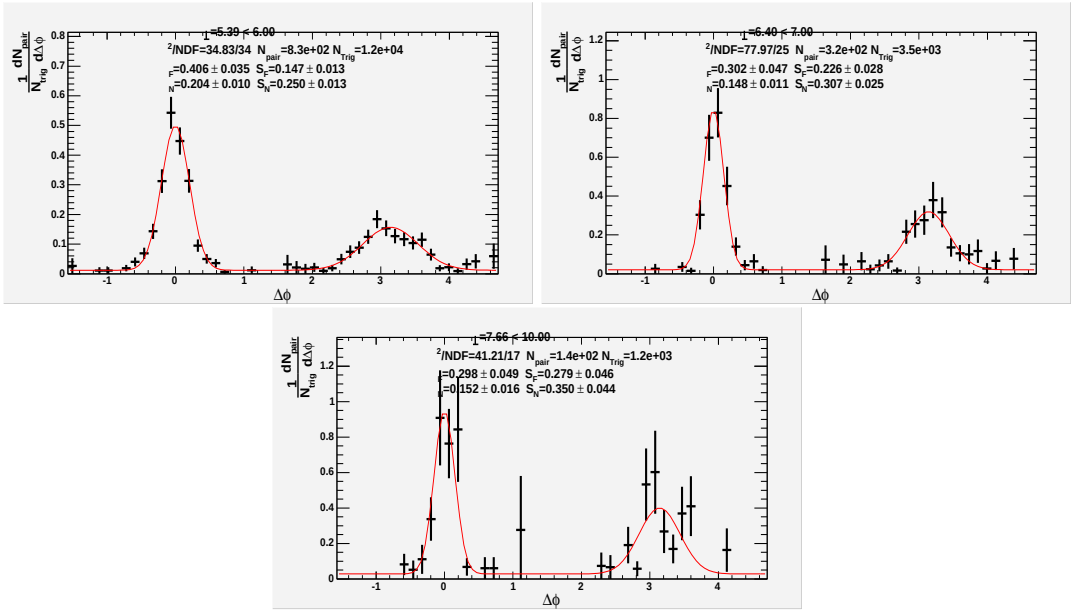

Figure 31: $\pi^0 - h^{\pm}$ p+p conditional yield distributions for a constant hadron p_T of 2-5 GeV/c. The fit is given by Equation 5. A table of extracted widths is given in Table 17.

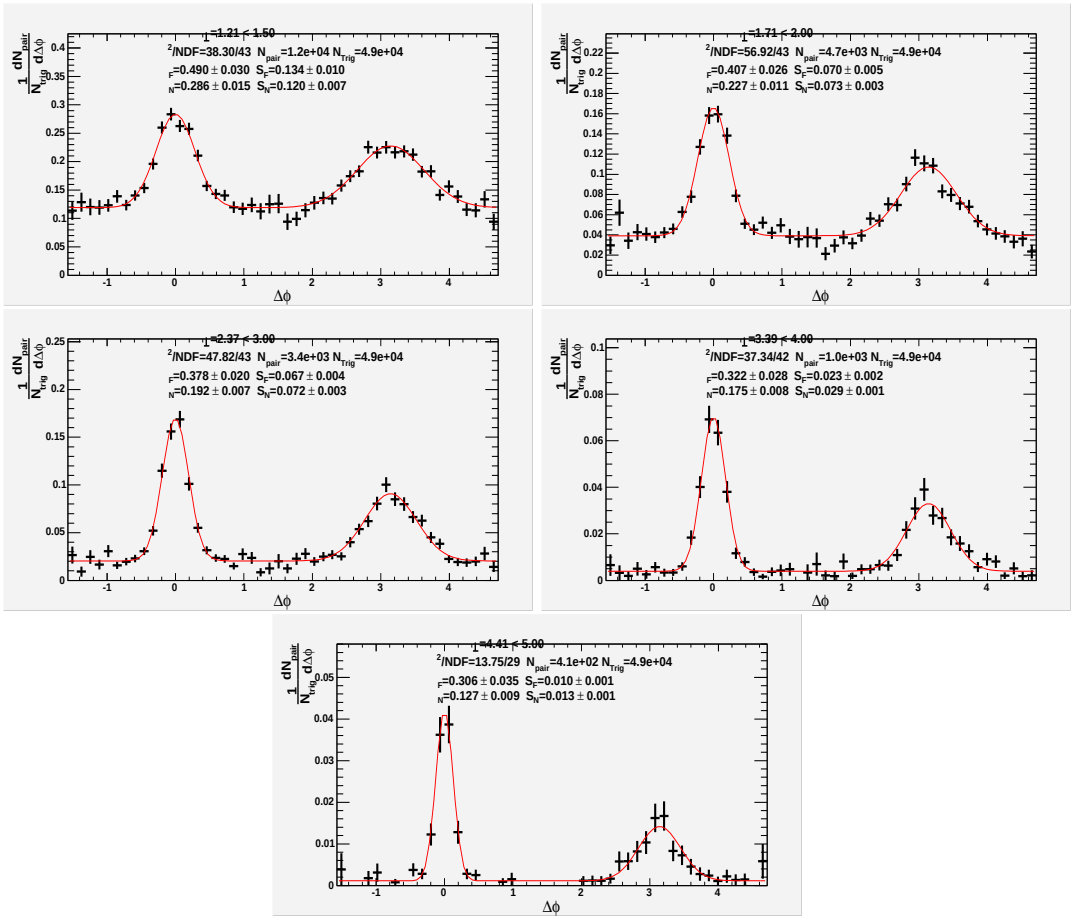

Figure 32: Constant π^0 trigger $\pi^0 - h^{\pm}$ p+p conditional yield distributions. The fit is given by Equation 5. Shape and yield results are given in Tables 18 and 19.

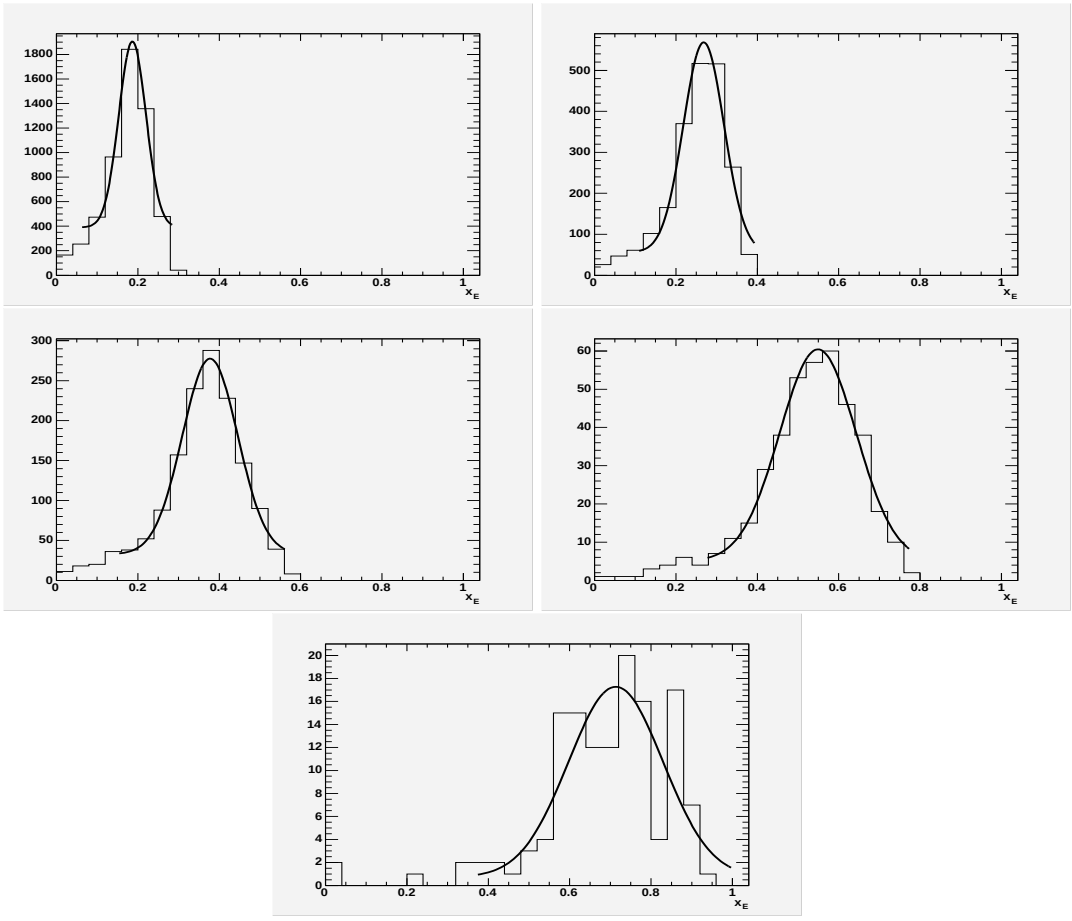

Figure 33: Constant π^0 trigger $\pi^0 - h^{\pm}$ p+p x_E distributions. The fit is a gaussian plus a flat term. x_E results are given in Table 19.

H Tables of Values for Jet Shapes and Yields for p+p $\pi^0 - h^{\pm}$ Correlations with Fixed Associated Hadron

$p_{T,trig}$	$\sigma_N(rad)$	$\sigma_F(rad)$	$\langle\|j_{Ty}\|\rangle$	$\langle z\rangle\langle\|k_{Ty}\|\rangle$
5.394	$0.207 \pm 0.007 \pm 0.009$	$0.409 \pm 0.025 \pm 0.013$	$0.395 \pm 0.014 \pm 0.026$	$1.031 \pm 0.083 \pm 0.043$
6.398	$0.151 \pm 0.008 \pm 0.006$	$0.304 \pm 0.034 \pm 0.010$	$0.297 \pm 0.016 \pm 0.020$	$0.936 \pm 0.136 \pm 0.038$
7.658	$0.144 \pm 0.012 \pm 0.006$	$0.295 \pm 0.035 \pm 0.009$	$0.291 \pm 0.024 \pm 0.019$	$1.091 \pm 0.169 \pm 0.044$

Table 17: Near and Far angle widths extracted from p+p $\pi^0 - h^{\pm}$ correlations with a constant hadron p_T of 2-5 GeV/c ($\langle p_{T,assoc}\rangle = 2.697$ GeV/c).

I Tables of Values for Jet Shapes and Yields for p+p $\pi^0 - h^{\pm}$ Correlations with Fixed Trigger π^0

$p_{T,assoc}$	$\sigma_N(rad)$	$\sigma_F(rad)$	$\langle\|j_{Ty}\|\rangle$	$\langle z\rangle\langle\|k_{Ty}\|\rangle$
1.209	$0.299 \pm 0.017 \pm 0.012$	$0.540 \pm 0.037 \pm 0.017$	$0.276 \pm 0.015 \pm 0.019$	$1.314 \pm 0.150 \pm 0.084$
1.715	$0.230 \pm 0.011 \pm 0.009$	$0.480 \pm 0.038 \pm 0.015$	$0.299 \pm 0.015 \pm 0.020$	$1.282 \pm 0.133 \pm 0.075$
2.382	$0.204 \pm 0.009 \pm 0.009$	$0.430 \pm 0.031 \pm 0.014$	$0.355 \pm 0.016 \pm 0.023$	$1.191 \pm 0.102 \pm 0.068$
3.401	$0.167 \pm 0.007 \pm 0.007$	$0.321 \pm 0.026 \pm 0.012$	$0.387 \pm 0.017 \pm 0.026$	$0.892 \pm 0.089 \pm 0.055$
4.405	$0.129 \pm 0.009 \pm 0.006$	$0.345 \pm 0.040 \pm 0.014$	$0.360 \pm 0.026 \pm 0.026$	$1.014 \pm 0.131 \pm 0.064$

Table 18: Near and Far angle widths extracted from p+p $\pi^0 - h^{\pm}$ correlations with a constant π^0 p_T of 5-10 GeV/c. ($\langle p_{T,trig}\rangle = 5.756$ GeV/c)

$p_{T,assoc}$	x_E	dN_{near}/dp_T	dN_{far}/dp_T	dN_{near}/dx_E	dN_{far}/dx_E
1.209	0.189 ± 0.041	$0.360 \pm 0.020 \pm 0.038$	$0.462 \pm 0.038 \pm 0.054$	$2.071 \pm 0.116 \pm 0.217$	$5.676 \pm 0.465 \pm 0.664$
1.715	0.274 ± 0.053	$0.181 \pm 0.009 \pm 0.019$	$0.254 \pm 0.020 \pm 0.027$	$1.042 \pm 0.053 \pm 0.109$	$2.385 \pm 0.191 \pm 0.255$
2.382	0.382 ± 0.077	$0.112 \pm 0.005 \pm 0.012$	$0.118 \pm 0.008 \pm 0.012$	$0.643 \pm 0.026 \pm 0.068$	$1.531 \pm 0.107 \pm 0.161$
3.401	0.565 ± 0.073	$0.049 \pm 0.003 \pm 0.005$	$0.037 \pm 0.003 \pm 0.004$	$0.281 \pm 0.015 \pm 0.029$	$0.514 \pm 0.047 \pm 0.054$
4.405	0.701 ± 0.138	$0.019 \pm 0.002 \pm 0.002$	$0.020 \pm 0.002 \pm 0.002$	$0.111 \pm 0.009 \pm 0.012$	$0.143 \pm 0.017 \pm 0.015$

Table 19: Near and Far yield and x_E distirbutions extracted from p+p $\pi^0 - h^{\pm}$ correlations with a constant π^0 p_T of 5-10 GeV/c. ($\langle p_{T,trig}\rangle = 5.756$ GeV/c)

References

[1] AN #257

[2] AN #228

[3] AN #263

[4] J. Jia's note on $\pi^{\pm}$

[5] AN #210

[6] AN #251

[7] AN #283